Formation of the giant Aynak copper deposit, Afghanistan: evidence from mineralogy, lithogeochemistry and sulphur isotopes

Hamidullah Waizy, Norman R. Moles, Martin P. Smith & Adrian J. Boyce

Taylor & Francis
Taylor & Francis Group

Formation of the giant Aynak copper deposit, Afghanistan: evidence from mineralogy, lithogeochemistry and sulphur isotopes

Hamidullah Waizy[a,b], Norman R. Moles [ID][a], Martin P. Smith[a] and Adrian J. Boyce[c]

[a]School of Environment and Technology, University of Brighton, Brighton, UK; [b]Department of Geological Engineering and Exploration of Mines, Faculty of Geology and Mines, Kabul Polytechnic University, Kabul, Afghanistan; [c]Isotope Geoscience Unit, Scottish Universities Environmental Research Centre (SUERC), Glasgow, UK

ABSTRACT

Aynak is the largest known copper deposit in Afghanistan, with indicated resources of 240 Mt grading 2.3% Cu placing it in the 'giant' category. Host rocks are Neoproterozoic metasediments comprising dolomitic marble, carbonaceous quartz schist and quartz-biotite-dolomite schist containing garnet, scapolite and apatite. Chalcopyrite and bornite dominate the hypogene ore with lesser pyrite, pyrrhotite, cobaltite and chalcocite, and rare sphalerite, molybdenite, uraninite and barite. Sulphides occur as bedding-parallel laminae, disseminations, metamorphic segregations and crosscutting veins. Sulphide δ^{34}S ratios range −14.5 to +17.3‰ in bedded and disseminated sulphides (n = 34). This broad range favours biogenic reduction of seawater sulphate as a major source of sulphur, although thermochemical reduction processes are not precluded. The narrower δ^{34}S range of −6 to +12.2‰ in vein and segregation sulphides (n = 21) suggests localized redistribution and partial homogenization during metamorphism. Geochemical associations suggest that Al, P, Ca, Ti and Fe were primary sedimentary constituents whereas Cu, Mg, S, Se, As, Co and Bi were introduced subsequently. We infer that Aynak originated as a shale- and carbonate-hosted stratabound replacement deposit, resembling orebodies of the Central African Copperbelt, although underlying red-beds are absent at Aynak and mafic volcanics were the probable copper source. These giant deposits formed worldwide in the Cryogenian probably due to marine enrichment in copper, magnesium and sulphate coincident with profuse basaltic volcanism and ocean oxidation.

1. Introduction

The timing of mineralization, the sources of fluids and migration pathways, the sources of metals and of sulphur, and sulphide precipitation mechanisms have been points of contention in studies of stratabound ore deposits globally (e.g. Kirkham 1989; Wilkinson 2014; Sangster 2018). Interpretations are divided between syngenetic and epigenetic models, though copper introduction during diagenesis has been favoured for many sediment-hosted copper sulphide deposits (e.g. Hitzman et al. 2010). Textural relationships between ore and host rock minerals are critically important in deducing paragenesis and establishing the relative timing of ore formation (e.g. Craig and Vokes 1993; Fontbote et al. 2017). However, the study of metasediment- and metavolcanic-hosted stratabound ore deposits is more complicated as recrystallization during metamorphism may have progressively erased fine-scale textural features that would otherwise have provided evidence for ore-forming processes, and metamorphic fluids may have redistributed

ore constituents which then precipitated in structurally controlled locations (e.g. Cartwright and Oliver 2000; Marshall et al. 2000; Marignac et al. 2003; Zheng et al. 2013; Zhong et al. 2015; Turlin et al. 2016). Further confusion results from semantic issues over the terms syngenetic, epigenetic, and diagenetic.

Where metamorphic processes have complicated the interpretation of ore genesis, whole-rock geochemical associations may be informative, for example through establishing likely sedimentary protoliths (e.g. Chisonga et al. 2012) or quantifying element associations produced by alteration and replacement processes (e.g. Large et al. 2001; Bailie and Gutzmer 2011; Zhang et al. 2018). Several studies have demonstrated that metamorphic re-equilibration of sulphides at low to medium metamorphic grades results in only micrometre or millimetre scale homogenization of δ^{34}S values (Crowe et al. 1990; Velasco et al. 1998; Giacometti et al. 2014) with pre–metamorphic δ^{34}S variations commonly being preserved at least on a scale larger than individual mineral grains. Sulphur isotope ratios are also useful as they can

provide constraints on sulphide deposition mechanisms, particularly the involvement of biogenic or thermogenic reduction of dissolved sulphate (e.g. Gustafson and Williams 1981), and sulphur sources in terms of basinal, magmatic or metamorphic fluid (e.g. Mandeville 2010; Shanks 2014). That said, modern sulphate-reducing bacteria can produce fractionations that span a huge range of $\delta^{34}S$ values from 0 to over 70‰, largely dependent on the availability of porewater sulphate (Rickard 2012).

This paper presents mineralogical, mineral textural and geochemical research that provides insights to processes that formed the Aynak giant copper deposit in Afghanistan (Figure 1(a)). Afghanistan is endowed with major resources of copper with around 300 documented deposits and occurrences in host rocks ranging from Proterozoic to Neogene in age, including sediment–hosted, skarn, porphyry, and vein–hosted mineralization (MOMP and AGS 2014). Around 94 of these, including the Aynak deposit, are located in the Kabul Copper District, an area of 800 square kilometres situated within the fault-bound Kabul Block (Figure 1(b,c)). Here, sulphide mineralization occurs mainly in metasedimentary sequences that have been subjected to low – to medium–grade regional metamorphism. The inferred protoliths are mixed carbonate–siliclastic shallow marine sediments deposited in intracratonic basins (AGS and BGS 2005a). Located about 30 km SSE of Kabul in Logar Province, the Aynak deposit has been exploited by artisans for over 2400 years: the Mes Aynak site contains remnants of an ancient settlement with former smelting furnaces visible at the surface along with extensive slag from former production. Following re-discovery in the 1970s and extensive drilling, a team of Afghan and Soviet geologists defined a broadly tabular orebody up to 210 m thick underlying an area of ca 6 square kilometres, divided into two prospects namely Central Aynak and Western Aynak (Figure 2). Published accounts (AGS and BGS 2005b; MOMP and AGS 2014) give a drill-indicated resource of 660 million tons (Mt) at an average grade of 1.67% Cu, or 240 Mt at 2.3% Cu using a cut-off grade of 0.4% Cu, although the Soviet-era resource calculations do not conform to modern classifications and the resource estimate includes small ore lenses which may not be economically mineable. At present (2020), the Central deposit is awaiting development by the Ministry of Mines and Petroleum of Afghanistan (MoMP) and the Metallurgical Corporation of China (MCC). Our study is based entirely on unweathered rock, sampled from deep boreholes that penetrate below the ca 100 m thick oxidation and supergene enrichment zone. Our aim is to consider evidence for primary ore-forming processes in the metasediments and, based on the inferred genetic model, to place constraints on the mineralizing processes which may be important in mine development and exploration for further resources.

2. Geological setting of the Aynak copper deposit

The stratigraphy in the vicinity of the ore field comprises metamorphosed sedimentary and volcanic rocks, subdivided into the Welayati, Loy Khwar and Gulkhamid Formations. Their sedimentation age, though not well constrained, is considered to span from the late Neoproterozoic to the Lower Cambrian (Ludington et al. 2007). These 'basement' rocks are partially overlain by Upper Permian and Neogene sedimentary rocks and Quaternary sediments that fill a wide erosion–tectonic depression. Also occurring in the area are various intrusive rocks, assigned to three complexes according to their age and composition: a Late Proterozoic ('Riphean') complex of small intrusions of sub-alkaline composition; an Ediacaran–Cambrian mafic dyke complex; and a Lower Cretaceous complex of ultramafic rocks (AGS and BGS 2005b). The following description of the main stratigraphic units, starting with the oldest, is summarized from reviews by AGS and BGS (2005a, 2005b) and Ludington et al. (2007) and previous geological survey reports translated into English by Craig (2013).

2.1. Welayati formation

Akocdzhanyan et al. (1977) divided the Welayati Formation into three main lithological units. The oldest unit occurs in the cores of anticlinal structures in the vicinity of the Aynak deposit (Figure 2) and more extensively north of Kabul City (Figure 3(a)). This comprises garnetiferous gneisses, amphibolitic gneisses and schists containing staurolite, andalusite and sillimanite. Collett et al. (2015) established that these rocks were metamorphosed to granulite facies followed by a subsequent amphibolite-facies overprint. Based on U-Pb dating of zircon and U-Th dating of monazite, Faryad et al. (2016) established a Paleoproterozoic age of ~1.85–1.80 Ga for the granulite facies metamorphism. At the top of this unit is an angular unconformity overlain by amphibolite facies basaltic–andesitic metavolcanic rocks with intercalations of quartzitic and carbonate schists. This unit is conformably overlain by further quartzitic, micaceous and carbonate schists that also record amphibolite facies
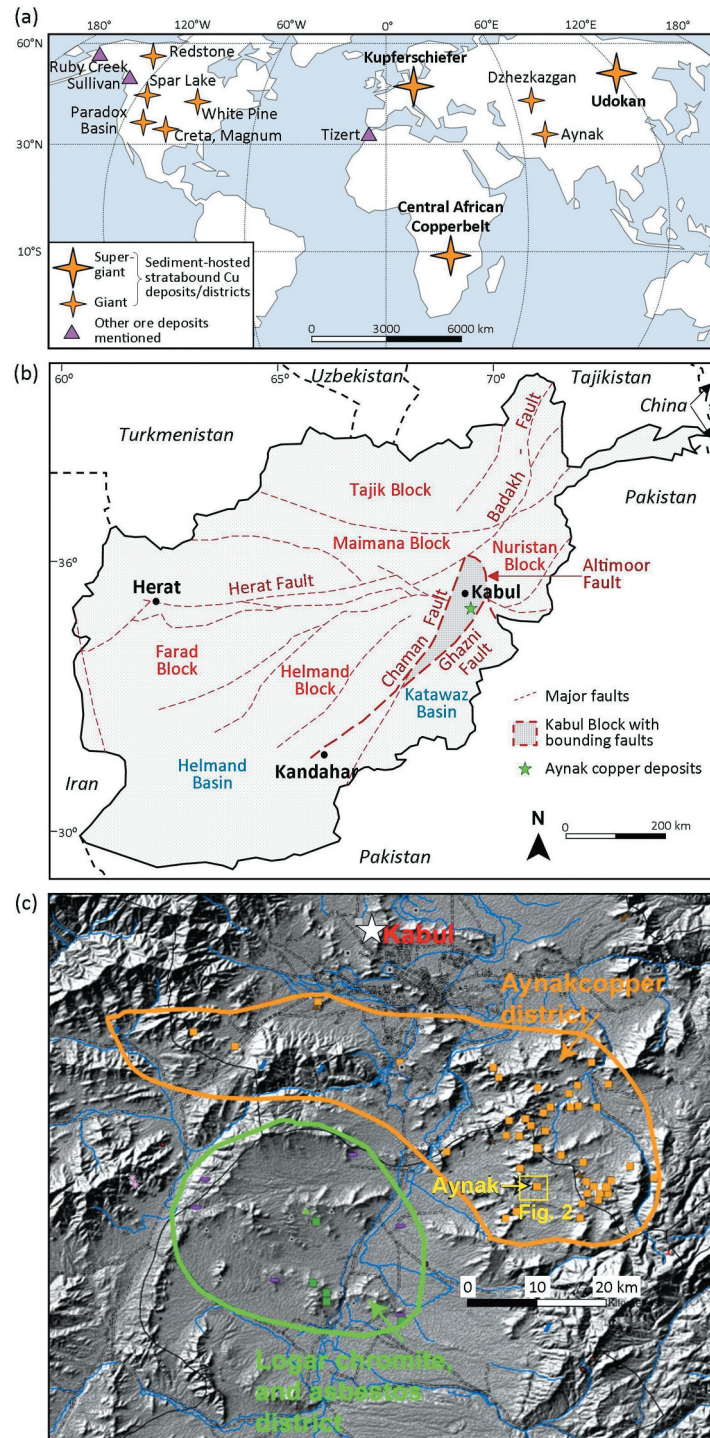
Figure 1. (a) Global distribution of giant sediment-hosted stratabound copper deposits and districts (adapted from figures in.Hitzman *et al.* 2010; Taylor *et al.* 2013), and of other ore deposits mentioned in the text. (b) Tectonic map of Afghanistan with locations of the Kabul Block and the Aynak copper deposits, modified from AGS and BGS (2005a). (c) Digital terrain model of the northern part of the Kabul Block superimposed with locations of mineralization, modified from MOMP and AGS (2014). Orange squares indicate sediment-hosted copper occurrences; the Aynak deposits are arrowed. Green squares indicate occurrences of chromite and asbestos in the Logar ultramafic complex. White star northwest of Kabul indicates location of the Khayakhana quarry (location details in Collett *et al.* 2015). Yellow box indicates the area shown in Figure 2.
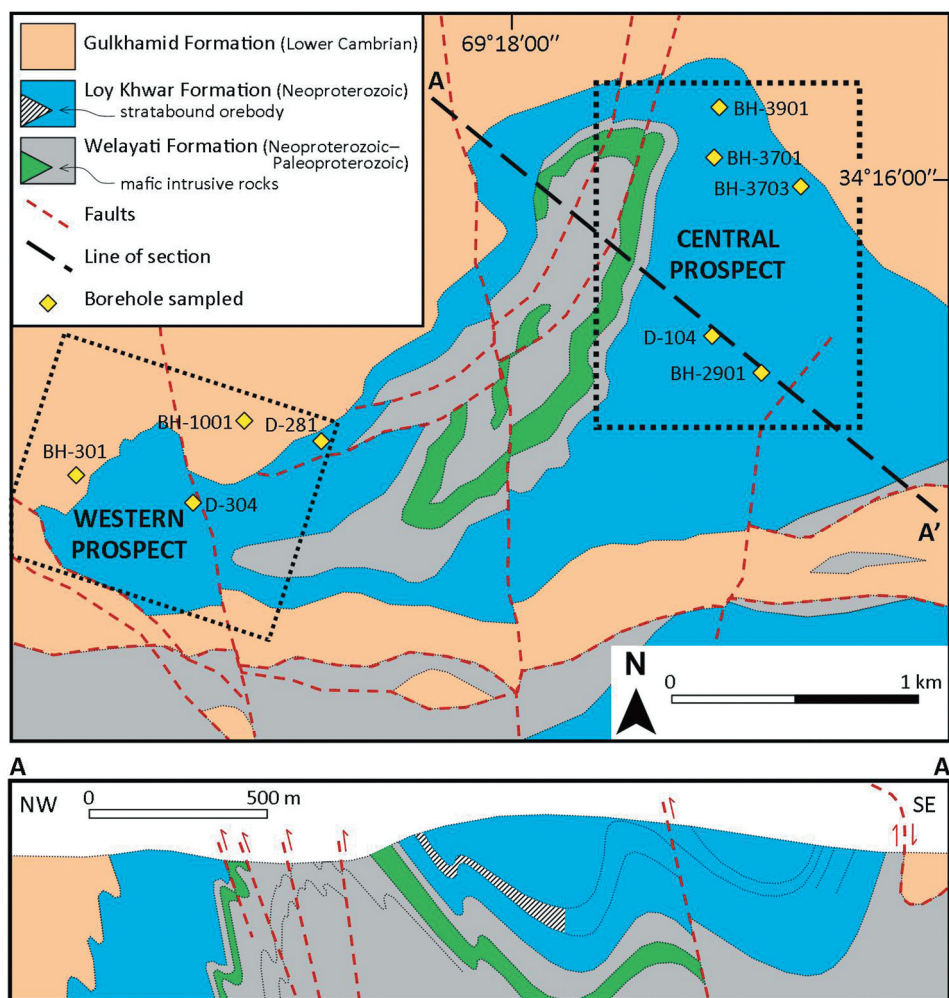
Figure 2. Simplified geological map and cross-section of the Aynak deposits, modified from AGS and BGS (2005a), showing the Central and Western prospect areas and locations of drillholes from which samples were obtained for this study (SM1 Tables 1 and 2).

metamorphism (Collett *et al.* 2015). Based on Ar-Ar dating of micas and U-Th dating of monazite, Faryad *et al.* (2016) established that the Upper Welayati Formation was metamorphosed during a widespread orogeny at around 850–900 Ma.

2.2. Loy Khwar formation: orebody host rocks

The orebodies are hosted in the Loy Khwar Formation which comprises a repetitive cyclical sequence of dolomite marble, carbonaceous quartz schist and quartz–biotite–dolomite schist (Figure 3(b,c)). The formation varies in thickness from 420 m in the Western prospect to 880 m in the Central prospect (Figures 2 and 4). The stratigraphy was characterized during the Afghan–Soviet exploration as reported by Gusev *et al.* (1979), who divided the formation into seven members plus several sub-members (Figure 4). Graphitic schist and dolomite marble commonly retain fine rhythmic layering inferred to be of

sedimentary origin, and the meta-evaporite mineral scapolite is reported in the Western prospect. Elsewhere in the Kabul Block, stromatolite remnants in the Loy Khwar Formation have been used to propose a Neoproterozoic age, although identification of the stromatolites formerly named 'Tannuofia' has been taken to suggest a Lower Cambrian age. Based on this evidence, the formation has been assigned to the Ediacaran–Cambrian (formerly Vendian–Cambrian: Mennesier 1961; Slavin *et al.* 1972; Feruz 1973; AGS and BGS 2005a).

In the previous Afghan–Russian studies (Yurgenson *et al.* 1981, translated in Craig 2013), two types of hypogene ore are distinguished: a bornite-type with secondary chalcocite that makes up the main ore bodies, and a chalcopyrite-type that is present above and below the main orebody (Figure 4). This rhythmic zoning is broadly conformable to the decimetric compositional layering of the sedimentary host rocks. The lower sections of the main orebody are hosted in carbonaceous dolomite–
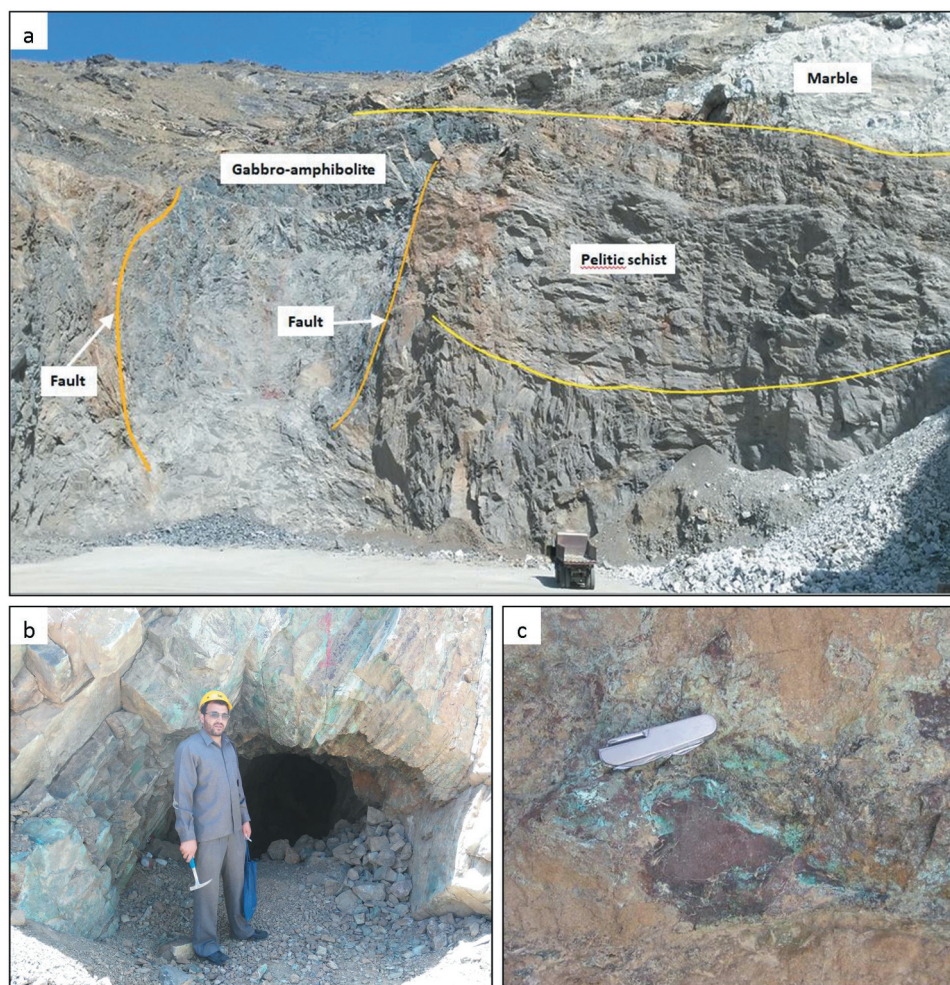
Figure 3. Rock exposure photographs. (a) Khayakhana quarry northwest of Kabul City (mining truck for scale), showing multiple episodes of deformation in the basement rocks. (b) Central Aynak adit showing malachite staining in steeply dipping beds of calcareous biotite schist and marble (first author for scale). (c) Close up of surface exposure in Central Aynak showing malachite supergene alteration in mineralized dolomitic marble (photograph from Benham et al. 2007).

quartz schist, in part breccia-textured, and these rocks contain chalcopyrite, pyrite and pyrrhotite with minor cobaltite and sphalerite (Yurgenson *et al.* 1981). The central–upper sections of the orebody are hosted in carbonaceous quartz–biotite schist, quartzites and dolomite marble. In these sections, the chief ore mineral is bornite, with lesser chalcopyrite and minor molybdenite, cobaltite and magnetite. The mineralization is dispersed through the host rocks as disseminations, laminae, lens-shaped segregations, and veinlets, and does not form discrete, laterally extensive mineralized beds of massive and laminated sulphides such as commonly found in 'sedimentary exhalative' deposits.

2.3. Gulkhamid formation, deformation and Phanerozoic cover

The Gulkhamid Formation conformably overlies the Loy Khwar Formation and is widespread in the Aynak area

reaching a thickness of 500 m. Only the lower part of the formation is preserved, mainly comprising gabbro-amphibolites and calcareous–biotite schists which represent a basic to intermediate volcanic protolith. The metavolcanic rocks host disseminated magnetite and lesser amounts of ilmenite, haematite and pyrite. The formation includes subordinate intercalations of metasedimentary rocks comprising dolomite marble, graphitic–quartz schists, and quartz-biotite-dolomite schist.

Following deposition of the Gulkhamid Formation, and Late Proterozoic to Early Cambrian intrusions of sub-alkaline bodies and a mafic dyke complex, regional metamorphism and associated tectonic deformation took place. The age of the metamorphism and tectonism is presumed to be post-Early Cambrian, and pre-Upper Permian, but is otherwise poorly constrained by geological relationships. In the vicinity of the Aynak deposits, the deformation produced a NNE-SSW-trending asymmetrical anticline structure (Figure 2) which exposes the
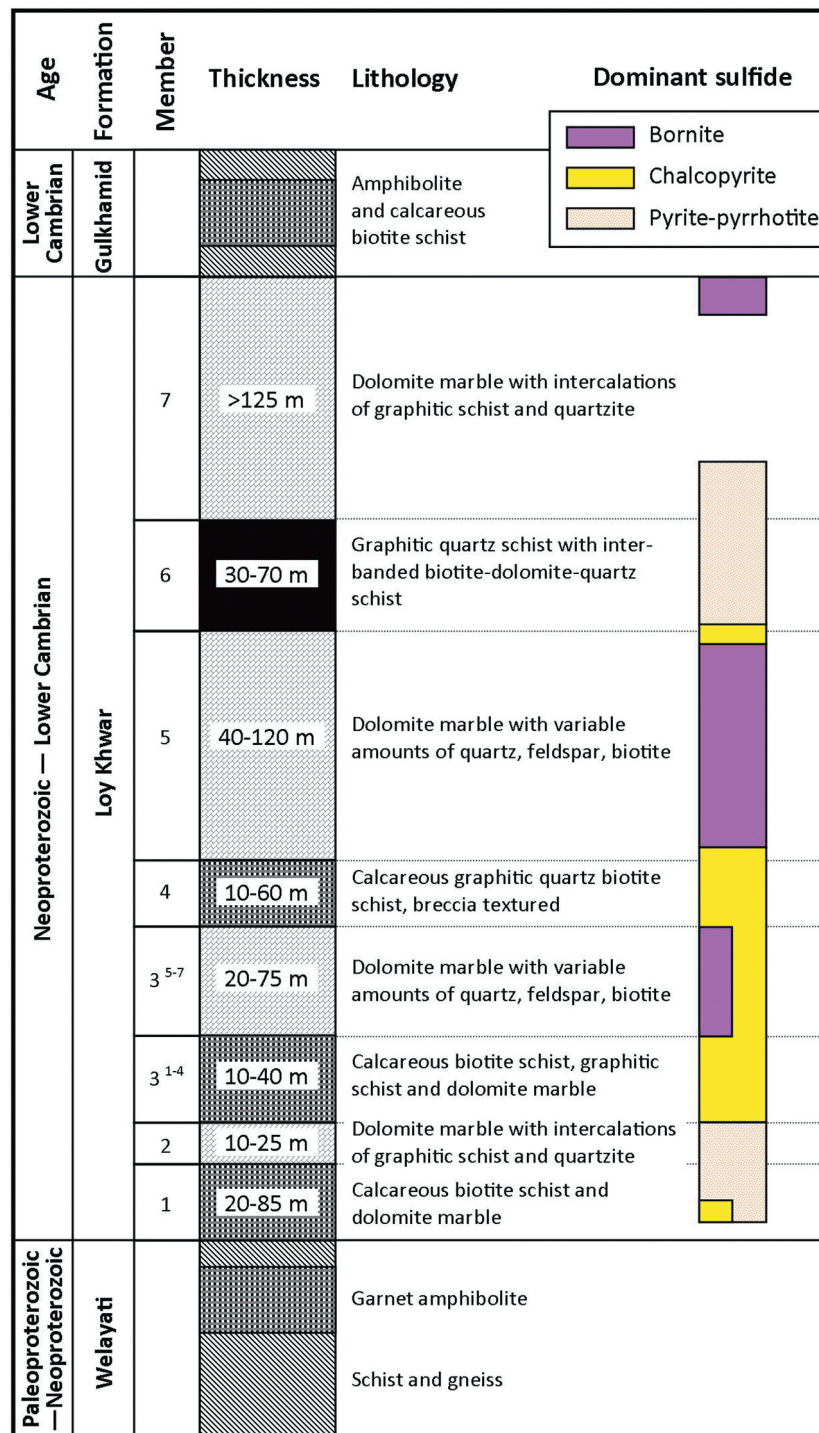
Figure 4. Generalized stratigraphic column, after MOMP and AGS (2014), showing the major rock types and sulphide mineral zonation in the Aynak deposit. Not to scale, as thicknesses differ within, and between, the Central and Western parts of the ore deposit.

Welayati Formation in the core with the Loy Khwar Formation and its mineralization on the eastern and western flanks. The Central Aynak prospect is located on the shallow-dipping eastern limb of the anticline and the Western Aynak prospect is on the more steeply inclined western limb.

Unconformably overlying the older rocks in the western and the southern part of the Aynak area are small outcrops of the Upper Permian Khingil Formation comprising horizontally bedded conglomerate and coarse sandstone. A Lower Cretaceous ultramafic complex occurs south of Aynak in the vicinity of Logar (AGS and

BGS 2005b), characterized by occurrences of chromite and asbestos (Figure 1(c)). At Aynak, most of the outcrop of the orebody is covered by poorly consolidated fluvial and fluvio–lacustrine deposits of Quaternary age, referred to as the Lataband Formation, which attains a thickness up to 600 m in the Central Aynak area.

3. Materials and methods

Samples of unweathered ore and host rocks were obtained from selected deep drillholes in the Central and Western parts of the Aynak deposit (Figure 2, Supplementary Material file SM1 Tables 1 and 2). A total of 47 small drillcore samples were recovered, each a few centimetres in size, of which 38 contained sulphides. In addition, five sulphide-bearing samples were collected from mafic rocks that outcrop with minimal oxidation in the Tara Khel location of the Khayarkhana area near Kabul Airport (Figure 1(c)). Polished thin sections were prepared, and optical and scanning electron microscopy (SEM) studies were undertaken to investigate petrographical characteristics and mineral compositions. A Zeiss EVO LS15 SEM with an Oxford Instruments Aztec energy dispersive X-ray spectrometer (EDX) employing an 80 mm X-max detector was used at the University of Brighton. SEM-EDX results are presented in Supplementary Material file SM1.

Semi-quantitative whole-rock geochemical analyses were obtained for 40 samples using XRF methods (Van Gaans *et al*. 1986). Flat sawn surfaces of drillcore samples were tested using an Olympus Innov-X Delta Professional (DPO-2000) hand-held XRF analyser. For each sample, at least three measurements each of 60-s duration were obtained from different facets and averaged, taking further measurements of heterogeneous samples. This procedure was preferred to crushing and grinding the drillcore samples due to their small size and to avoid destruction. Semi-quantitative elemental data for 27 elements were generated: results are presented in Supplementary Material file SM2. To calibrate the output to international reference standards, appropriate normalization factors were applied separately to analyses of the carbonate- and silicate-rich rocks. In all analyses, Co and Hg concentrations were below the instrumental detection limit of 0.004%. As XRF analysis cannot distinguish Fe^{2+} and Fe^{3+}, total Fe is expressed as $Fe_2O_3{}^t$ even though some or much of the iron occurs as sulphides. Where element concentrations were below the XRF detection limits, numerical values of half of the estimated detection limit for each element were applied for the purpose of Principal Components Analysis of the geochemical datasets (Supplementary Material file SM2 Table 3).

For sulphur isotope geochemistry, 2–5 g representative samples of sulphide minerals, mainly pyrite, chalcopyrite and bornite, from the Aynak orebodies and Khayarkhana area were handpicked under a binocular microscope from partially crushed core samples. Sulphide–rich separates were treated with acetic acid to remove any associated carbonate minerals. Some drillcore samples contained more than one textural occurrence of sulphides (bedding parallel, disseminated, segregated, and cross-cutting veins), in which case texture-specific subsamples were obtained (Supplementary Material file SM3). Pure sulphide samples were powdered before 5–10 mg aliquots were taken for sulphur isotope analysis using conventional bulk analysis methods at the Scottish Universities Environmental Research Centre (SUERC) isotope facilities in East Kilbride, Scotland. Standard techniques (Robinson and Kusakabe 1975) were utilized in which SO_2 gas was liberated by combusting the sulphides with Cu_2O as an oxidizing agent at 1025°C in an evacuated furnace. Purified SO_2 was analysed on a VG isotech SIRA II mass spectrometer and standard corrections were applied to raw $\delta^{66}SO_2$ values to produce the true $\delta^{34}S$ values (Robinson and Kusakabe 1975). Data precision and accuracy were monitored using repeat analyses of international and internal standards (Lipfert *et al*. 2007) namely NBS–123 = +17.1‰, IAEA–S–3 = − 31.5‰ and CP–1 = − 4.6‰. Repeat analyses of these standards provide $\delta^{34}S$ values of NBS–123 = +17.2‰, IAEA–S–3 = − 31.9‰ and CP–1 = − 4.57‰ respectively with a standard error around ±0.2‰ during the analyses of these samples. Values are reported (SM3 Table 3) in $\delta^{34}S$ notation as per mil (‰) variations from the Vienna Cañon Diablo Troilite (V–CDT) standard.

4. Results

4.1. Host rock mineralogy and mineral chemistry

Metamorphic textures dominate the Aynak ore and host rocks with schistose fabrics in non-graphitic mica-bearing rocks, and coarsely crystalline carbonates and sulphides in some carbonate-rich rocks (Figure 5). Graphitic mica schists, quartzites and some dolomitic marbles have fine-grained textures and small-scale lithological variations (Figure 5) that are suggestive of bedding. In fine-grained rocks, parallel disseminations and laminations of sulphides may be relict bedding features, or may be post-sedimentation features developed parallel to the bedding planes.

The main rock-forming minerals in the host rocks are carbonates, quartz, micas, and plagioclase feldspar, with scapolite in some samples. Carbonates are ubiquitous,
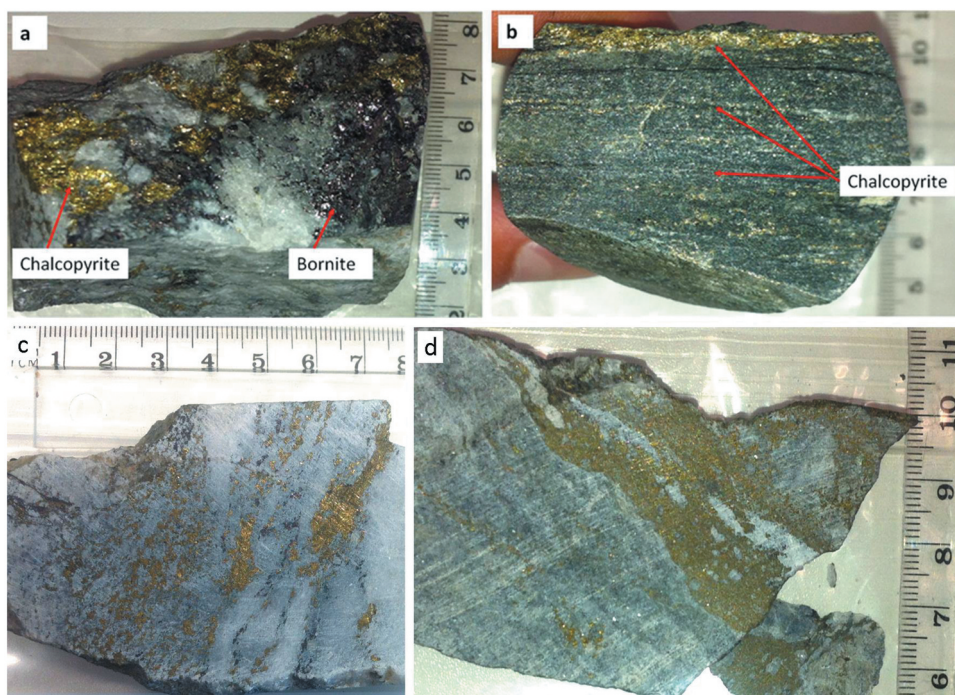
Figure 5. Samples of drillcore from the Aynak deposits illustrating the typical mineralogy and textural features of ore and host rocks: (a) coarse segregations of chalcopyrite, bornite and quartz in quartz-dolomite marble sample 281–3; (b) bedding-parallel laminae and disseminations of chalcopyrite in dolomite marble sample 3901–2; (c) fine-grained disseminated and vein-associated coarsely crystalline chalcopyrite and bornite in sulfidic marble sample 3703–3; (d) chalcopyrite bedding-parallel lenses and disseminations in dolomitic marble sample 301–3.

and are dominated by ferroan dolomite. In some samples dolomite forms relatively large crystals (0.5–5 mm) but fine-grained dolomite rocks are more typical (Figures 5 and 6). Calcite is a major component of dolomitic marble. In other lithologies, minor quantities of calcite commonly occur in cross-cutting veinlets, either as the only vein-forming mineral or accompanied by quartz and rarely pyrite, bornite and chalcopyrite. SEM-EDX analyses of carbonate minerals (n = 60: Supplementary Material file SM1) indicate that calcites contain up to 1.5 wt% Mn, 1 wt% Fe and 0.8 wt% Mg and dolomites contain 1.7–8.6 wt% Fe and up to 2.1 wt% Mn. No significant differences were found in the compositions of calcite and dolomite in samples from Central and Western Aynak. Siderite, found only in sample 104–4a, contains 6–8 wt% Ca, 2–4 wt% Mg and 0.5 wt% Mn. Ankerite containing 9 wt% Mg and 2 wt% Mn was found as a very minor constituent of dolomite-rich sample 304–2.

Quartz forms the fine-grained matrix (typically 10–100 µm) to quartz-rich metasediments as well as coarsely crystalline aggregates (typically 0.5–2 mm, up to 20 mm) in metamorphic segregations and veins in association with dolomite, bornite and chalcopyrite (Figure 6(a,b)). Fluid inclusions are common in coarsely crystalline quartz which consequently appears milky

white in hand specimens. These veins are interpreted as late-metamorphic 'Alpine' fissure-type veins (i.e. generated by localized pressure-solution and re-precipitation) whereas fine-grained quartz generally occurs in the host rocks and is interpreted as originating from pre-existing sedimentary material. The ubiquitous presence of micron-sized inclusions of graphite and sulphides, which inhibit recrystallization during metamorphism (Carlson 2011), may account for the maintenance of finely crystalline quartz in the metasediments.

Biotite, phlogopite and muscovite are common in the host rocks, particularly in the quartz mica dolomite schist units. In Western Aynak, phlogopite is the principal mica rather than biotite which is dominant in Central Aynak. Biotite in sulphide-rich rocks has higher Mg/Fe ratios than in the host schists, probably due to the preferential partitioning of iron into iron-bearing sulphides and ferroan dolomite during diagenesis and/or metamorphism (cf. Raiswell *et al*. 2011).

Plagioclase in the compositional range andesine–oligoclase–albite commonly occurs in quartz–feldspar and feldspar–carbonate host rocks (Figure 6(e,f)). Scapolite was observed optically as a major component (modal proportion ~30%) in Western Aynak samples 301–5 and 1001–3 (Figure 6(g,h) and Figure 7(i)). EDX
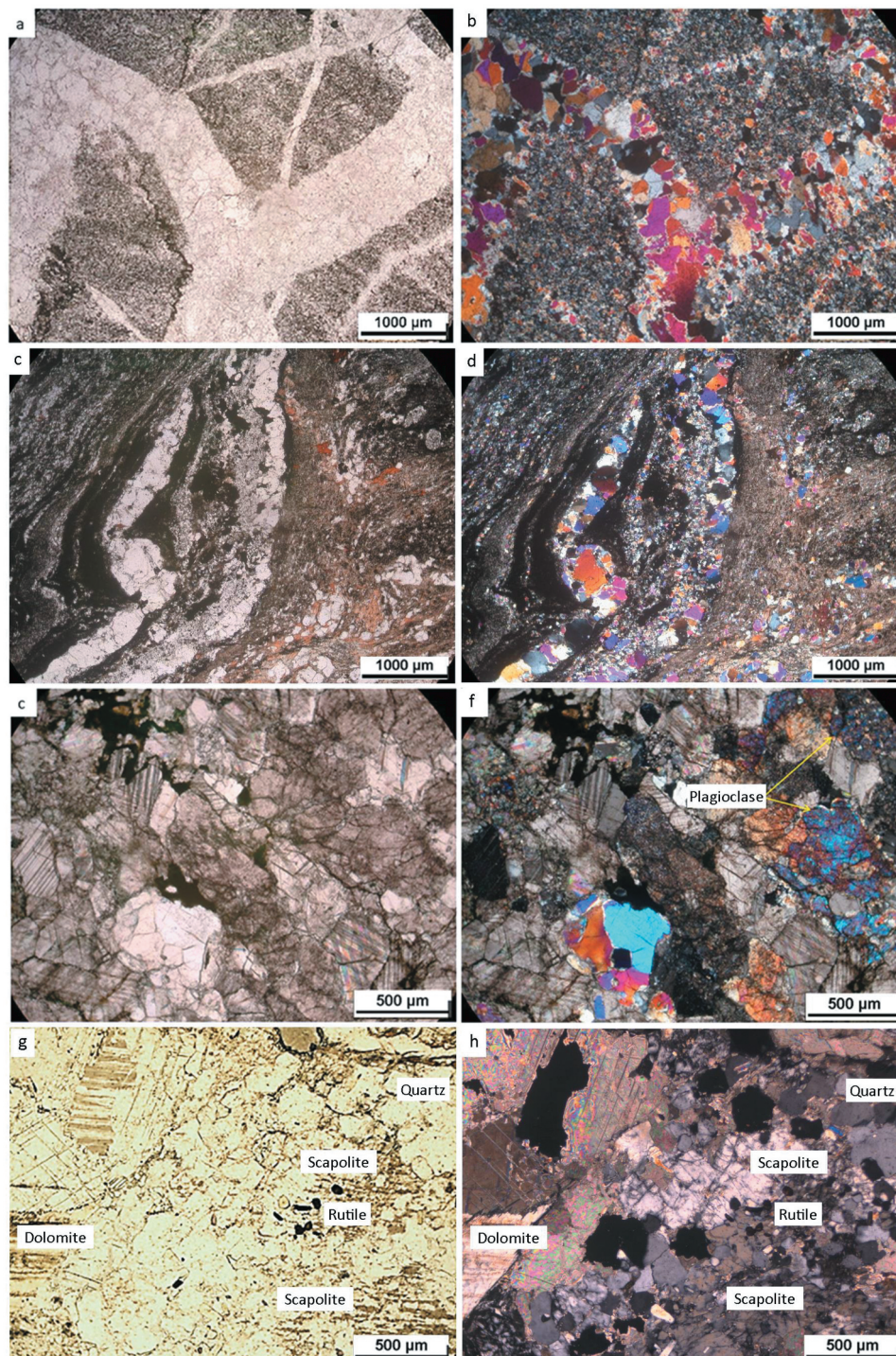
Figure 6. Transmitted light photomicrographs of Aynak drillcore samples: (a) and (b) plane–polarized and crossed-polar images of sample 304–3a, showing fine-grained quartz in the metamorphosed sedimentary rock and coarsely crystalline quartz in veins; (c) and (d) plane–polarized and crossed-polar images of sample 304–2, a fine-grained, crenulated schist comprising quartz, carbonates and micas (mainly biotite), with minor chalcopyrite and pyrite, and bedding-parallel quartz veins; (e and f) plane–polarized and crossed-polar images of sample 104–1, a siliceous marble comprising carbonates, quartz and plagioclase, with minor sulphides (chalcopyrite and pyrite); (g and h) plane–polarized and crossed-polar images of sample 1001–3, a dolomitic marble containing scapolite and apatite.

analyses (n = 4) of scapolite in 1001–3 indicate compositions ranging from $Na_{1.99}Ca_{1.89}Al_{4.30}Si_{7.70}O_{24}Cl$ to $Na_{2.56}Ca_{1.36}Al_{4.01}Si_{7.99}O_{24}Cl$. Up to 0.6 wt% potassium is present but sulphur was not detected. Although carbonate ion contents are not determined by this analytical method, they are likely to be low considering
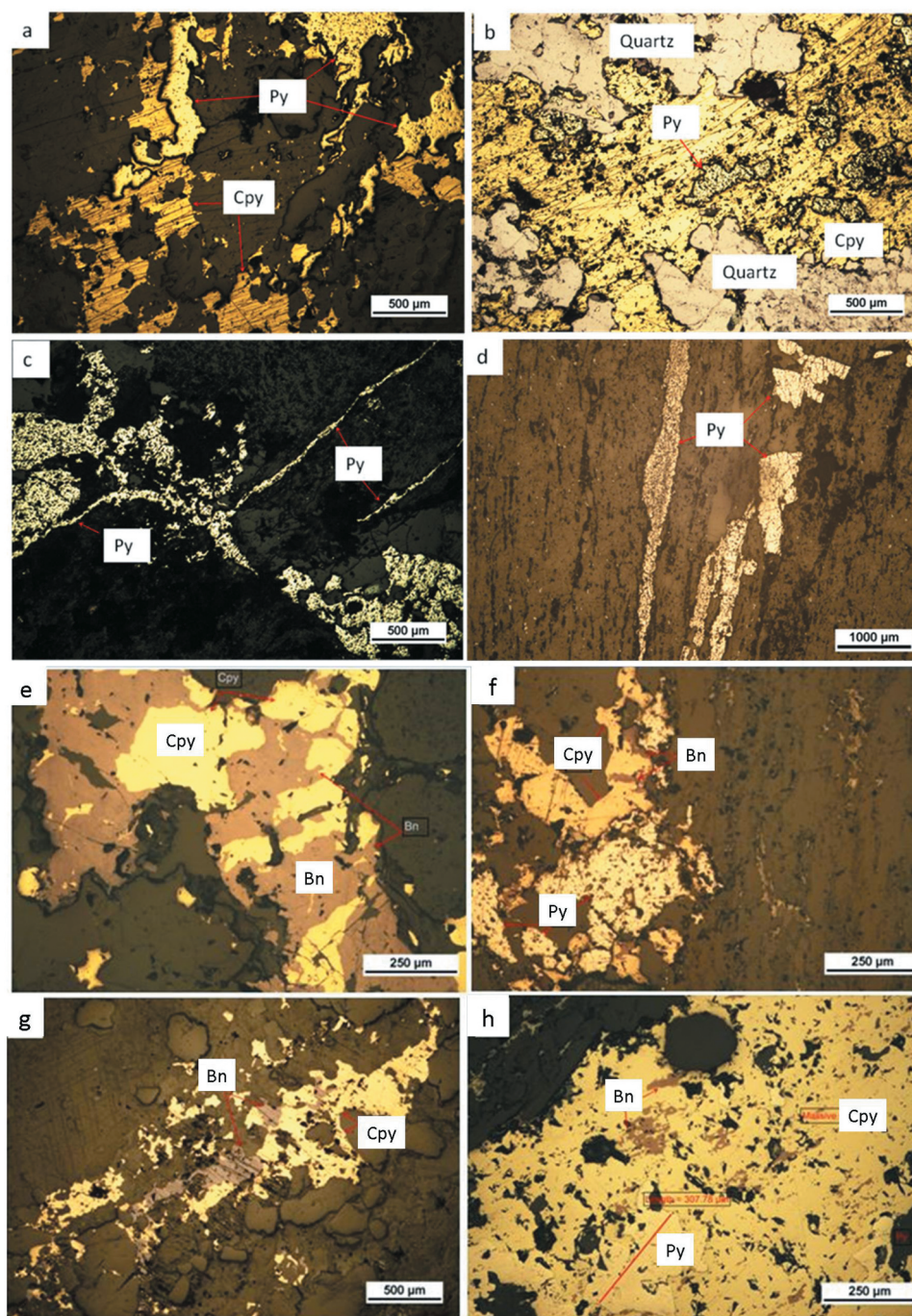
Figure 7. Reflected light photomicrographs of Aynak drillcore samples: (a) and (b) chalcopyrite and pyrite interspersed with dolomite and quartz, in sample 301–4; (c) patchy and cross-cutting pyrite veins in sample 1001–2; (d) fine- and coarsely crystalline pyrite occurring as bedding-parallel aggregates in sample 3901–1; (e) intergrown bornite and chalcopyrite (possibly bornite replacement of chalcopyrite), in sample 3703–3a; (f) replacement of porous-textured pyrite and bornite by chalcopyrite in sample 3703–4; (g) subordinate bornite in chalcopyrite, possibly due to exsolution, in sample 301–3; (h) pyrite and bornite replacement by chalcopyrite, in sample 304–2.

the relatively high chlorine contents of 2.1–3.1 wt%. If this presumption is valid, the scapolite is dominated by the marialite ($Na_4Al_3Si_9O_{24}Cl$) component with a lower fraction of the meionite ($Ca_4Al_6Si_6O_{24}CO_3$) component (Deer et al. 2004).

Apatite occurs widely as small disseminated crystals within the host rocks and with chalcopyrite and pyrite in veins and segregations. It is a major component of Western Aynak sample 281–1, forming almost mono-minerallic bands (Figure 8(c,d)). SEM-EDX
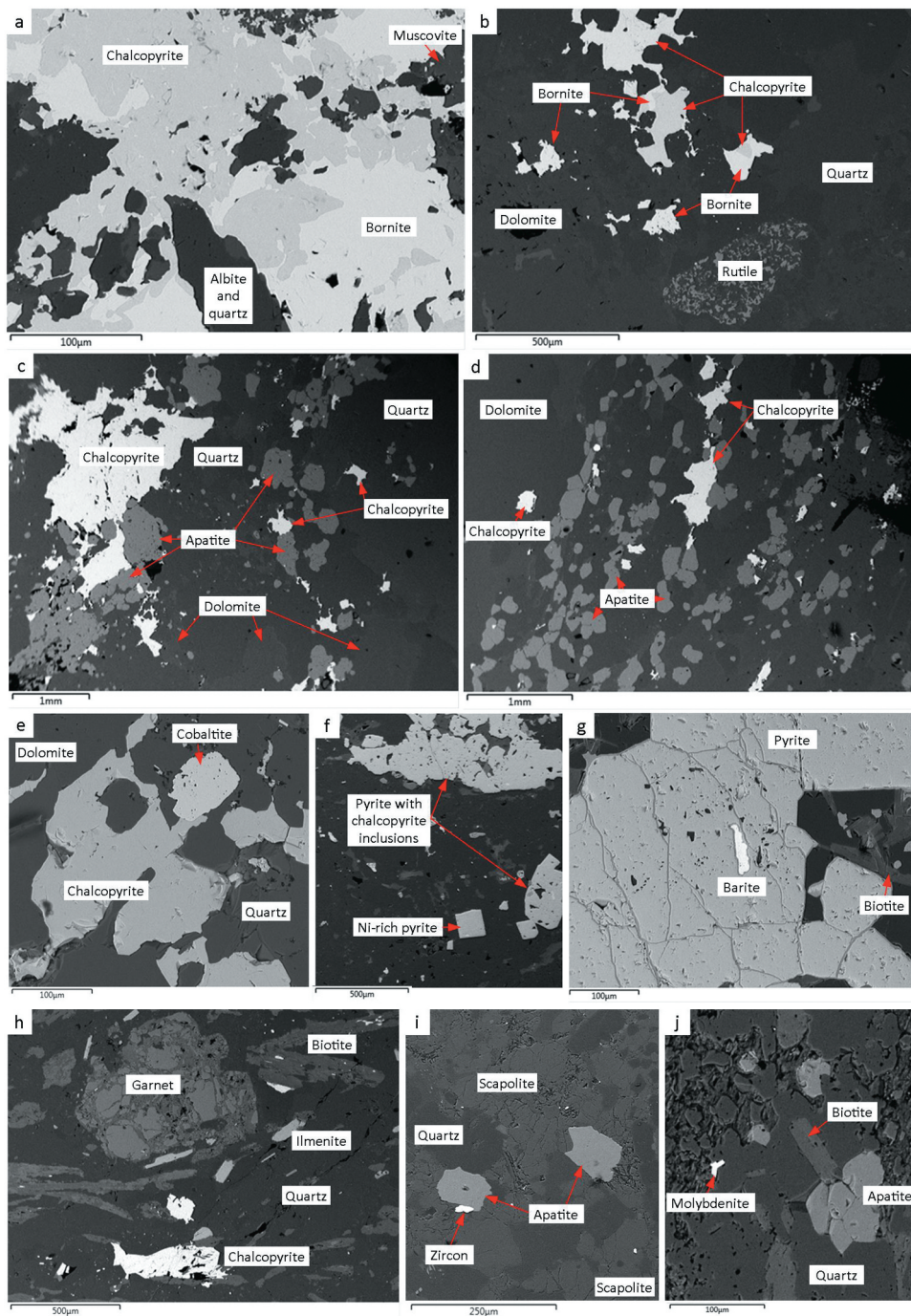
Figure 8. SEM back-scattered secondary electron images of Aynak drillcore samples: (a) intergrown bornite and chalcopyrite, with carious texture and relict islands of bornite suggesting partial replacement by chalcopyrite, in sample 301–3; (b) carious-textured bornite and chalcopyrite with sieve-textured rutile grain in quartz–dolomite schist sample 281–2; (c) and (d) high modal abundance of apatite with chalcopyrite as disseminated grains and coarse segregations in quartz–dolomite schist sample 281–1; (e) cobaltite with chalcopyrite in marble sample 2901–4; (f) inclusion-rich pyrite with overgrowths and separate crystals of inclusion-poor euhedral pyrite in schist sample 3901–1; (g) barite inclusion within inclusion-rich core of coarse pyrite aggregate in sample 3901–1; (h) garnet crystal wrapped around by the quartz-biotite matrix containing ilmenite and chalcopyrite in schist sample 281–5; (i) scapolite and apatite in sample 1001–3; (j) small crystals of molybdenite in sample 304–4.

analyses (n = 52) show that Aynak apatite is predominantly fluorapatite with 2.0–3.5 wt% F and 0–1.0 wt% Cl. Central Aynak samples generally have lower

chlorine contents and lower Cl/F ratios (0–0.32) than Western Aynak samples (ratios up to 1.13). The highest chlorine concentrations, up to 2.1 wt%, occur in

scapolite-bearing Western Aynak samples 1001–3 and 301–5, in which the apatite has about equal wt% F and wt% Cl.

Garnet occurs rarely in the host rocks (SM1 Table 2). In Western Aynak sample 281–5, EDX analysis of a garnet crystal 0.5 mm in diameter (Figure 8(h)) indicates a composition intermediate between almandine and spessartine–grossular with a minor pyrope component. The garnet is partially replaced by chlorite. Chlorite has also partially or completely replaced biotite in some samples. This replacement suggests retrograde metamorphic hydration reactions, which may also account for patches of fine-grained white mica (sericite) partially replacing feldspars.

In addition to the main rock-forming minerals, minor quantities of rutile, ilmenite, titanite, magnetite, haematite and zircon were observed in samples studied microscopically. Small crystals of monazite, allanite, thorite, uraninite and xenotime were observed under SEM. Rutile is the most widespread of the titanium minerals, followed by ilmenite and lesser amounts of titanite. Rutile occurs equally commonly in sulphide rocks and in unmineralized host rocks. It forms skeletal, sieve-like crystals in one sample (Figure 8(b)). Whereas in most samples the composition is close to pure TiO_2, in sample 301–3 rutile contains up to 1.5 wt% Nb and 0.5 wt% Fe, and in sample 1001–2 rutile contains up to 1.2% V. Ilmenite is widespread in small amounts in host rock and ore samples (e.g. Figure 8(e,h)). Compositions determined by SEM-EDX analyses (n = 23) range from $(Fe_{0.8} Mn_{0.2})TiO_3$ to $(Fe_{0.92} Mn_{0.08})TiO_3$ with the highest Mn in Central Aynak sample 3901–3. Titanite occurs in four samples variously as inclusions, in the rock matrix, and within cross-cutting veins. SEM-EDX analyses indicate compositions close to stoichiometric $CaTiSiO_5$.

Finely dispersed graphite, or in some samples the carbonaceous substance shungite, occurs in dark-grey dolomite marble and in carbon-quartz-biotite schist. A biogenic origin is indicated by carbon isotope analyses of material extracted from three samples ($\delta^{13}C$ range – 22.4 to – 23.8 ‰), and Raman spectra indicate that some carbonaceous material is less than full ordered graphite (John Parnell, personal communication, 2019). Four spectra all show distinct G peaks, with less distinct and less intense D and D' peaks. Spectral characteristics were compared to the kerogen and graphite fields of Wopenka and Pasteris (1993) and this comparison confirmed that the Aynak samples comprise graphite consistent with the relatively high grade of metamorphism (Muirhead *et al*. 2016).

4.2. Sulphide (and sulphate) mineralogy and mineral chemistry

The mineralogy of the sulphide ores of Aynak is relatively simple, although complicated by metamorphism and at shallow depths by weathering and supergene alteration. The hypogene sulphide minerals are, in order of decreasing abundance, bornite and chalcopyrite, pyrite, cobaltite, chalcocite, pyrrhotite, sphalerite and molybdenite. Minor amounts of carrollite, smaltite and pentlandite were reported by previous researchers but not confirmed in this study.

Based on the set of samples studied, bornite is the most abundant copper mineral in the Central Aynak prospect where it usually forms compact planar or dispersed aggregates several millimetres in size that lie roughly parallel to interpreted bedding planes. In metamorphic segregations and veins, aggregates and individual crystals of bornite can be up to several centimetres in size (Figure 5(a)). Under microscopic examination, bornite and chalcopyrite are commonly intergrown (Figure 7(e–h)) and in some cases, carious textures indicate partial replacement of bornite by chalcopyrite (Figure 8(a)). Trellis exsolution of chalcopyrite (cf. Li *et al*. 2018) is often seen in the bornite, which reflects incident light with an anomalous yellowish tint, possibly due to forming partial solid solutions with chalcopyrite and digenite (Yund and Kullerud 1966). However, 20 SEM-EDX analyses indicate that Aynak bornite approximates to the stoichiometric composition Cu_5FeS_4 with no substituting elements detected. Where bornite and pyrite occur in close proximity, they show textural evidence for partial replacement by chalcopyrite (Figure 7(f, h)) (Yund and Kullerud 1966).

Chalcopyrite is the principal hypogene copper mineral in the studied samples from the Western Aynak prospect. As with bornite, chalcopyrite occurs mostly as disseminations and segregations, but also as bedding-parallel layers (Figure 5(b)) and as the matrix in some brecciated rocks. SEM-EDX analyses show no significant variation from the stoichiometric formula $CuFeS_2$. In the supergene alteration zone, chalcopyrite is partially or completely replaced by bornite, chalcocite, cuprite, native copper and malachite (Figure 3(b,c)). Chalcocite is rare in hypogene ore where it occurs exclusively as intergrowths within bornite.

Pyrite occurs in subordinate amounts in low-grade chalcopyrite ore and is absent from high-grade dominantly bornite ore. Pyrite is more common in strata overlying and underlying the copper-rich formations (Figure 4). In some cases, pyrite appears to have partially replaced chalcopyrite (Figure 7(a)). More commonly, an early pyrite phase is partially replaced by chalcopyrite as

evidenced by remnant islands of pyrite with carious grain boundaries (Figure 7(b)). Pyrite occurs within veins that lie parallel to and transverse to bedding (Figure 7(c)) and also as disseminated blebs or streaks that are usually oriented along bedding (Figure 7(d)). When disseminated in the host rocks, fine-grained pyrite (10–200 µm) is often inclusion-rich and anhedral, whereas in the veins, pyrite crystals are euhedral and up to 5 mm across. In some samples, inclusion-rich anhedral pyrite is apparently overgrown by euhedral, inclusion-free pyrite (Figure 8(f,g)). During SEM examination of Central Aynak sample 3901–1, a single blade of barite was found as an inclusion 80 µm in length within a pyrite crystal (Figure 8(g)). EDX analysis indicates that the barite contains 2.7 wt% Sr and 0.4 wt% Ca. Barite was not found in the rock matrix of this sample or in other samples from Aynak.

Pyrite analysed by SEM-EDX in 14 samples is mostly close to stoichiometric FeS_2, with only six of 45 analyses reporting Co and Ni above the 0.2 wt% detection limit. Nickel concentrations of 1.2 wt% and 2.4 wt% were found in individual pyrite crystals in Central Aynak samples 3703–4 and 3901–1 respectively (Figure 8(f)). Pyrite in sample 104–4a contains 1–4 wt% Co. In Western Aynak sample 1001–4, one analysis of pyrite has 9.3 wt% Co, although cobalt was not detected in other pyrites in the thin section. Arsenic was not detected by SEM-EDX in any pyrite. However, bulk geochemical analyses of sulphide separates show moderate enrichments in As, Ni and Co with median values of around 0.05 wt%, 0.1 wt% and 0.25 wt% respectively (Waizy 2018).

Pyrrhotite was recorded in previous studies as a characteristic mineral of members 1 and 2 of the Loy Khwar Formation (Figure 4). Pyrrhotite occurring as small crystals around 50 µm was positively confirmed by SEM examination in one sample of carbonaceous schist, 1001–2. However, pyrrhotite is common in association with pyrite as indicated by magnetism of particles induced by using a hand magnet for mineral separation. Porous–textured pyrite observed microscopically in some samples (e.g. Figure 7(f)) may have formed as an alteration of pyrrhotite during retrograde metamorphism (cf. Hall *et al*. 1987; Craig and Vokes 1993).

Cobaltite was observed in three samples (2901–3, 2901–4 and 304–3a) as irregular grains 0.1 to 1.5 mm in size associated with chalcopyrite (Figure 8(e)) in relatively low-grade or medium-grade disseminated chalcopyrite ore. SEM-EDX analyses show that the cobaltite is close to stoichiometric CoAsS with minor substitution of iron for cobalt (range 1.1–3.6 wt% Fe, average 1.9 wt% Fe in 10 analyses). Nickel was not detected.

Sphalerite with a grain size of 50–100 µm was noted in only one sample, 3901–2, where it accompanies
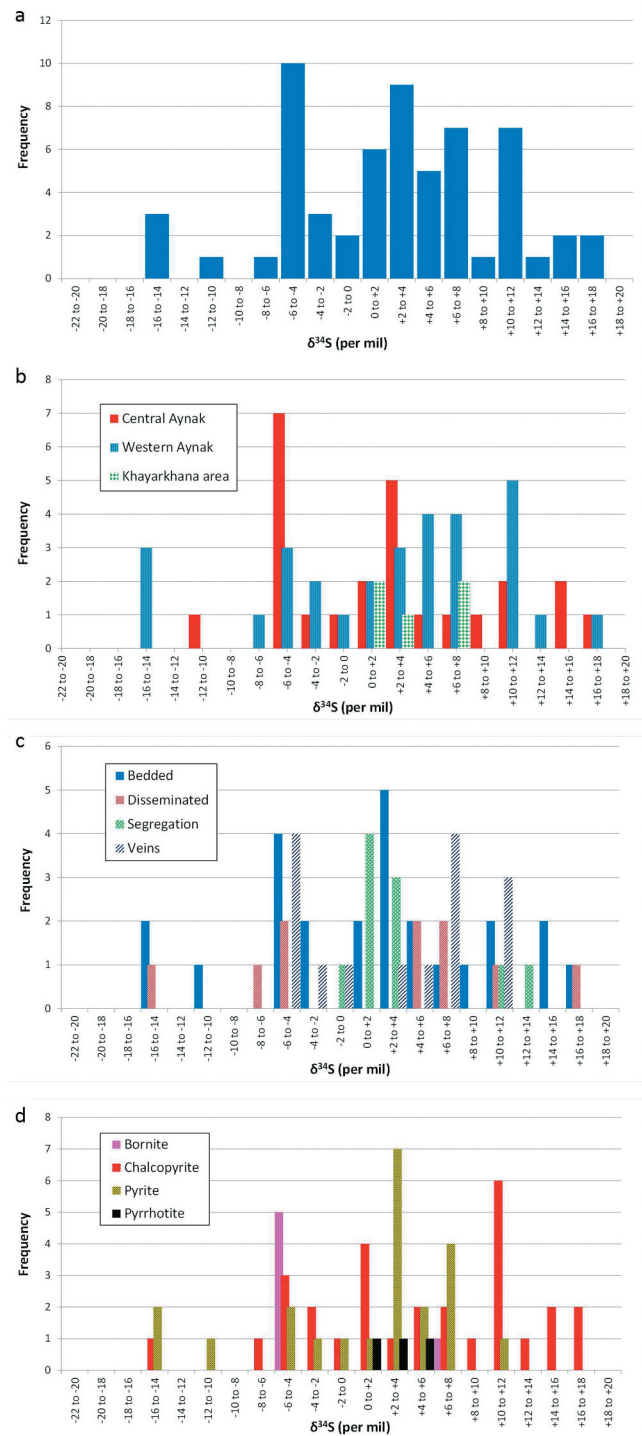
Figure 9. Sulphur isotope data (refer to SM3 Table 3): (a) all values obtained in this study; (b) sub–divided by locality; (c) sub–divided by textural association; (d) sub–divided by sulphide mineralogy.

chalcopyrite and pyrite. SEM-EDX indicates that the sphalerite contains ~6 wt% Fe. Molybdenite was found in two chalcopyrite-rich samples from Central Aynak. In sample 304–4, molybdenite forms irregular elongate grains around 30–50 µm in length (Figure 8(j)), associated with chalcopyrite, pyrite and cobaltite.
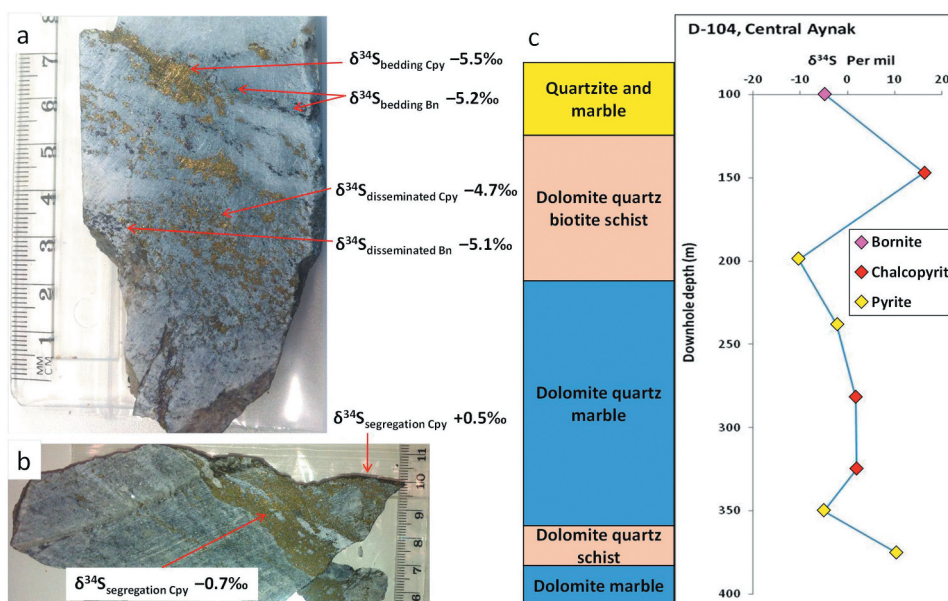
Figure 10. Millimetre to decametre-scale variations of $\delta^{34}S$ values and similarity in $\delta^{34}S$ values of adjacent bedding-parallel, disseminated and metamorphic segregation sulphides: (a) drillcore sample 3703–3, Central Aynak, showing bedding parallel and disseminated chalcopyrite and bornite with their $\delta^{34}S$ values; (b) drillcore sample 301–3, Western Aynak, showing the $\delta^{34}S$ values obtained from two layers of segregated chalcopyrite; (c) $\delta^{34}S$ values of sulphide samples (symbol colour indicates sulphide species) plotted against down-hole depths and the dominant lithologies in borehole D-104, Central Aynak.

4.3. Sulphur isotope geochemistry

The variation of $\delta^{34}S$ values in Aynak sulphides was investigated on scales ranging from millimetric (e.g. exsolved mineral pairs, adjacent bedding-parallel and vein sulphides), centimetric (within the same core sample), metric (core samples metres apart in the same borehole) and kilometric (samples from various depths across the lateral extent of the deposit) (Figure 9, SM3 Table 3). Relatively narrow $\delta^{34}S$ ranges were found in sub-samples from the same core sample (Figure 10a,b) with one exception; in sample 3701–1, bedding-parallel pyrite (+2.5‰) has a distinctly different isotopic composition to nearby vein/segregation sulphides (–1.1‰) (SM3 Table 3). Much greater $\delta^{34}S$ variation is seen in metric-scale sampling over distances of tens to hundreds of metres (Figure 10(c)).

The $\delta^{34}S$ results for the full set of analysed samples, shown in Figure 9(a), shows a broad range from –14.5 to +17.3‰. Plotting the sulphide data from the two major parts of the Aynak copper deposit, as shown in Figure 9(b), also reveals broad ranges of $\delta^{34}S$ values in each part (–10.4 to +16.2‰ (n = 25) for Central Aynak; –14.5 to +17.3‰ (n = 30) for Western Aynak). Sulphide $\delta^{34}S$ values obtained from contrasting structural settings proximal and distal from faults also show broad ranges; the values are not constrained to the spatial location of the boreholes or the vertical location of the samples within boreholes (SM3 Table 3). Three of the strongly negative $\delta^{34}S$ values were obtained from a single borehole (D–304) located in Western Aynak, and one was obtained from a borehole (D–104) located in Central Aynak; these two boreholes are central within the main mineralized zones in the respective areas.

Specific sulphide minerals also exhibit wide-ranging $\delta^{34}S$ values, as shown in Figure 9(d), with the highest positive (+17.3‰) and the lowest negative (–14.5‰) obtained from chalcopyrite samples. Pyrite shows a similarly wide range. Little significance should be attributed to the limited isotopic ranges found in bornite and pyrrhotite as relatively few samples of these minerals were analysed. As shown in Figure 9(c), a wide range of $\delta^{34}S$ values is exhibited by sulphides in contrasting textural contexts, although metamorphic segregations and veins show relatively small ranges compared to bedding-parallel and disseminated sulphides. Sulphides in metamorphic segregations have sulphur isotope values in the range –0.7 to +12.2‰ and these have the appearance of filling the compositional gap between the $\delta^{34}S$ values of disseminated and bedding-parallel sulphides.

Sulphides in samples from the Khayarkhana area show a relatively narrow span of $\delta^{34}S$ values in the range +1 to +7.8‰ (n = 5, SM3 Table 3). This contrasts with the wide range of values found in Aynak deposit sulphides (Figure 9(b)).

5. Discussion

5.1. Comparison of Aynak with other sediment-hosted copper deposits

Sediment-hosted stratiform copper deposits worldwide are typically hosted in intracratonic basins that formed at low latitudes, and which are commonly underlain by continental red-bed sediments (Brown 1997; Taylor et al. 2013). Red-beds are regarded by many authors as the source of oxidized fluids capable of transporting copper, and source of the copper itself, which may also be leached from volcanic rocks in the basal sedimentary sequence and/or the basement (e.g. Hitzman et al. 2005, 2010). However, red-bed sediments are not present in the stratigraphy underlying the Aynak deposit. Another difference is that carbonate rocks are a major component of the ore zone at Aynak (Figure 4) whereas in 'typical' sediment-hosted stratiform copper deposits, evaporites plus carbonate rocks and siliciclastic sediments stratigraphically overlie the mineralization where they are regarded as providing a hydrological seal to circulating ore-forming brines. Rupturing of the evaporite seal by basin-inversion-driven halokinesis is invoked by Hitzman et al. (2005) to account for sulphide precipitation at higher stratigraphic levels in Kansanshi and other Central African Copperbelt deposits.

In many sediment-hosted copper deposits, ore-grade mineralization is best developed along basin margins adjacent to basement highs (Selley et al. 2005; Hitzman et al. 2010). We do not have sufficient structural data for the Aynak deposit to evaluate this control. However, it is noteworthy that the Central and Western ore zones are located on the limbs of an anticlinal structure (Figure 2) with considerable lateral thickness variations in the host metasediments, which locally retain evidence of former evaporite beds. We speculate that the anticline axis may have been the site of a basement palaeo-high during deposition of the Loy Khwar Formation.

Further characteristic features of sediment-hosted copper deposits are mineralized envelopes that are transgressive to lithological boundaries and stratigraphic zonation of sulphide mineralogy, as clearly seen in the Kupferschiefer and Central African Copperbelt deposits (Kirkham 1989; Brown 1997; Hitzman et al. 2005; Muchez and Corbella 2012). It is difficult to ascertain whether mineralization is transgressive to lithological boundaries in the Aynak deposits due to an absence of marker beds and the abundance of vein-type mineralization within carbonate and siliciclastic metasediments. However, stratigraphical zonation in sulphide mineralogy is clearly evident in the Aynak deposits (Figure 4) comprising a central bornite-rich zone grading outward to chalcopyrite-rich and external pyrite-pyrrhotite zones. This zonation is typical of sediment-hosted copper deposits, as seen for example in the Ruby Creek (Bornite) Cu-(Co) deposit in Alaska (Bernstein and Cox 1986; Hitzman et al. 1986) and the Tizert Cu-Ag deposit in Morocco (Oummouch et al. 2017) (Figure 1 (a)). A possible explanation for this zonation is the replacement (within the ore zone) of early-formed framboidal pyrite by Cu-Fe sulphides. The timing of this replacement is considered in the next section.

Brown (2017) quantitatively modelled the Eh-pH conditions conducive to forming sediment-hosted copper deposits, and demonstrated that recirculation of reduced formation water would be incapable of transporting sufficient Cu to form giant deposits. Haematite-bearing red-beds, commonly invoked as a deep source of oxygen for late diagenetic to epigenetic fluids transporting Cu, are according to Brown not capable of producing Eh levels corresponding to those necessary to transport significant copper. Instead, his modelling favours Cu transport by the downward infiltration of copious amounts of oxygenated meteoric water enriched in evaporite-derived salts. In the Aynak copper deposits, Cu-enriched oxygenated waters were likely derived from the interaction of externally derived oxidized fluids (meteoric or evaporite-interacted) with overlying and/or underlying, magnetite-bearing mafic volcanic rocks (Figures 2 and 3(a)), as envisaged by AGS and BGS (2005a). Occurrences of marialitic scapolite and Cl-rich apatite in the ore and host rocks are consistent with the former presence of halite or of evaporite-assimilated fluids. Fluid inclusion results presented by Waizy (2018) for quartz in sample 104–5, Central Aynak, indicate high salinities with 30–50 equivalent wt% NaCl.

5.2. Timing of mineralization relative to sedimentation, diagenesis and metamorphism

The paragenetic sequence of hypogene mineralization in the Aynak deposits is difficult to reliably discern due to textural and mineralogical changes associated with regional metamorphism. Consequently, we discuss the timing of copper sulphide formation in relation to the deposition of the sedimentary host rocks, and the duration of mineralizing processes, reported in studies of other sediment-hosted copper deposits, before we discuss geochemical and mineralogical evidence for ore genesis at Aynak.

Copper mineralization may accrue in several episodes during the sedimentary-tectonic evolution of host basins (e.g. Selley et al. 2005) and, in particular deposits, the copper enrichment may be predominantly early diagenetic, late burial diagenetic, or synorogenic. Given constraints on the Eh evolution

of porewater and amount of copper capable of being transported in solution in oxidized brines (e.g. Brown 2017), a lengthy duration of fluid flow and/or multiple episodes of flow are essential for giant and supergiant copper deposits to form (Hitzman *et al*. 2010). In some giant deposits, such as White Pine in the USA (Figure 1(a)), textural features link mineralization with early diagenetic bacterial sulphate reduction (Brown 1971, 1997). Later diagenetic introduction of copper is probable where the paragenetic sequence exhibits textural evidence of replacement of framboidal-textured, early diagenetic iron sulphides by copper sulphides, such as recorded by Hitzman *et al*. (1986) at Ruby Creek and by Ommouch et al. (2017) at Tizert, and envisaged here for the Aynak deposits based on features described in section 4.2.

In the Ruby Creek Cu-(Co) deposit, petrographic studies (Bernstein and Cox 1986; Hitzman *et al*. 1986) suggest that bornite and most chalcopyrite formed late in the paragenetic sequence, whereas Re-Os analyses by Selby *et al*. (2009) indicate that at least some chalcopyrite precipitated during an early stage of mineralization associated with dolomitization. Re-Os chronology genetically links the Ruby Creek copper sulphide mineralization to volcanogenic massive sulphide deposits elsewhere in the same sedimentary basin, suggesting that regionally extensive hydrothermal activity was related to magmatism associated with continental rifting (Hitzman *et al*. 1986; Selby *et al*. 2009). We envisage that a similar scenario in the Kabul Block led to the formation of the Aynak copper deposits.

Conversely, in other sediment-hosted copper deposits, textural features and sulphide Re-Os dating indicate that mineralization is post-lithification and structurally controlled (for example in the Central African Copperbelt: McGowan *et al*. 2003; Cailteux *et al*. 2005; El Desouky *et al*. 2008; Sillitoe *et al*. 2010; and Nussir in northern Norway; Perelló *et al*. 2015). Consequently, these deposits have been interpreted as epigenetic in origin and attributed to fluid circulation during or after orogenic deformation and metamorphism. As noted by Selley *et al*. (2005) and Hitzman *et al*. (2010), the wide range in sulphur isotope compositions and Re-Os ages in the Zambian deposits suggest a multistage history of sulphide precipitation; indeed, earlier authors regarded diverse sulphur isotope compositions as a characteristic feature of sediment-hosted copper deposits. Widely ranging U-Pb ages in uraninite also imply a protracted history of fluid flow in the Central African Copperbelt deposits (Hitzman *et al*.

2010). Conversely, Sillitoe *et al*. (2017) present Re-Os molybdenite age determinations from deposits across the Zambian Copperbelt that indicate a relatively short period of mineralization in the Cambrian associated with tectonic shortening in the later stages of the Lufilian Orogeny. Re-Os dating of sulphide separates from the Aynak orebodies is currently (2020) in progress and may illuminate the timing of mineralization.

5.3. Geochemical–mineralogical associations and spatial/stratigraphic variation

As mentioned earlier, whole-rock geochemical associations may help in deducing genetic processes. In this section we first consider bivariate and multivariate associations in the dataset of 40 XRF analyses (Supplementary Material file SM2), and then consider spatial and stratigraphic trends in the bulk geochemistry.

Al_2O_3 and K_2O show a moderate positive association (Figure SM2B-a) with the exception of a subset of samples in which high Al is not matched by high K due to the dominance in these samples of the K-poor aluminosilicates plagioclase and scapolite, instead of micas. SiO_2 and CaO show a significant negative association (Figure SM2B-b) attributed to mutual dilution of quartz (and other silicates) and carbonates (the constant sum effect: Skala 1979). A strong positive association between MgO and CaO (Figure SM2B-c) is consistent with the predominance of dolomite, although Mg also occurs in phyllosilicates in schistose rocks, and high-Ca low-Mg compositions are characteristic of calcite-rich marbles. MgO and $Fe_2O_3^t$ show no overall correlation (Figure SM2B-d), a feature attributed to the presence of several Fe-bearing minerals, both as metallic species (e.g. pyrite, chalcopyrite and bornite) and as gangue (e.g. ferroan dolomite, micas). However, the concentrations of $Fe_2O_3^t$ and TiO_2 show a moderate positive association (Figure SM2B-e). The association of Ti and Nb with aluminosilicate minerals is demonstrated by the positive correlations between Al_2O_3, TiO_2 and Nb (Figure SM2B-f). Considering that Ti and Nb are generally indicators of clastic sediment input and are seldom mobile in low-temperature hydrothermal fluids (e.g. citations in Mathieu 2018), we interpret the relatively constant Fe-Ti association as representing the sediment precursor, therefore precluding a substantial hydrothermal input of Fe.

Raiswell *et al*. (2011) demonstrate that the authigenic Fe component (Fe_{auth}) in shales enriched in iron during diagenesis can be estimated using a factor based on the ratio of total Fe (Fe_T) to Al in typical clastic and/or

igneous source rocks ($Fe_{auth} = [Fe_T - 0.53 * Fe_T]/Al$). Applying this factor to geochemical data for the Aynak core samples, and calculating the proportion of Fe_T considered to be authigenic (Supplementary Material file SM2), generates values ranging from 5% to 100% with a median of 15% Fe_{auth}. Twelve of the 40 samples (30% of the sample set) have Fe_{auth} proportions higher than 50%. In this subset, most of the iron is authigenic or hydrothermal in origin rather than derived from clastic sources.

Iron and sulphur, and copper and sulphur, are poorly correlated in the sample set (Figures SM2B-g and -h) which lends support to a genetic model, discussed below, whereby Cu plus other metals and sulphur have been introduced into the orebodies after deposition of the Fe-bearing sediment precursor. The low cobalt concentrations reported here accord with AGS and BGS (2005a) who quote grades of 0.004% and 0.013% Co for two parts of the Central Aynak deposit.

Commonly used alteration indices, such as Ishikawa AI and the chlorite–carbonate–pyrite index (Mathieu 2018) cannot be applied to the geochemical data set reported here, as the PXRF analyses do not include Na_2O and in several cases the MgO content is below detection limits. Furthermore these indices assume that carbonatization is an alteration process, whereas in the Aynak deposit carbonate and mixed carbonate-clastic rocks are interpreted to be components of the sedimentary sequence. The predominance of albitic plagioclase over K-feldspar in the Loy Khar Formation could be construed as indicative of diagenetic alteration rather than hydrothermal alteration (cf. Large *et al.* 2001).

Multivariate associations in the dataset were investigated using Principal Components Analysis (PCA) (details in Supplementary Material file SM2). In the PCA for all analysed samples, due to compositional heterogeneity the first three components account for only 53% of variance, and therefore caution is needed in the interpretation of element associations as they may not be representative of the entire orebody. Variance is dominated by an inverse association (component 1, Figure SM2A-a) between elements associated with carbonates (Mg, Ca, Mn) and those associated with silicates (Al, K, Ti, V, Cr, Fe, Rb, Y, Zr and Nb). Cu and S enrichments are associated with trace element enrichments, notably Se and Bi, and are inversely correlated with Si content. Iron sulphides are represented by a geochemical association of Fe–Ni–S with associated Pb and Zn. However, as noted in the bivariate correlations, Cu and Fe have contrasting associations (Figure SM2A-a). Conversely, Fe–Ti–Al and associated high field strength trace elements (Y, Zr, Nb) are strongly correlated. Separate PCA runs of the geochemical data for

samples from Central and Western Aynak reveal some notable differences (Figures SM2A-b and -c), although interpretations are tentative given the small numbers of samples and their diverse compositions. In component 1, phosphorus is clearly associated with Mo, U and the carbonate component in Western Aynak whereas these associations are not evident in the Central Aynak dataset. Western Aynak component 4 and Central Aynak component 2 have similar element associations: copper sulphides with associated As, Se and Bi are clearly separated from the metals Ni, Zn and Pb. Iron (expressed as Fe_2O_3) plots in-between the element clusters representing silicates (micas) and Ni, Zn and Pb sulphides since Fe is a component of both assemblages. However, iron plots diametrically opposite to the copper sulphide cluster, again illustrating the inverse relationship between Fe and Cu in the sample sets.

Stratigraphic zonation in bulk rock geochemistry may reveal the effects of hydrothermal alteration within a stratabound orebody. Due to sampling restrictions, samples were collected from disparate locations within boreholes and it was not possible to investigate continuous geochemical variations. Nevertheless, major and trace element concentrations of the widely spaced samples were plotted to investigate any major changes with respect to stratigraphic position. In Central Aynak drillhole D–104 (Figure 2 and SM2C-a), Fe exhibits relatively constant concentrations, regardless as to whether Fe is incorporated into silicates or sulphides, as discussed above. Amongst the trace elements, Cu and S are very well correlated representing the Cu-rich sulphides. An exception is the peak for sulphur at the base of the profile which does not correspond to copper enrichment but instead represents iron sulphide enrichment, a feature consistent with the previously documented sulphide mineral zonation (Figure 4). Samples from borehole BH-301 in Western Aynak (Figure 2 and SM2C-b) show similar down-hole trends: Fe and Mg, as well as Al and K, are well correlated, suggesting the influence of micas in the major element geochemistry. Sulphur again shows a positive correlation with Cu reflecting the influence of Cu-bearing sulphides and poor correlation of Cu with other geochemical variables.

In order to investigate lateral variation of bulk geochemistry in Western Aynak, comparisons are made with sample geochemistry in borehole BH-1001 (Figure 2 and SM2C-c). The trends are similar to those observed in the shallower borehole BH-301, although comparative enrichment in K_2O in BH-1001 represents an overall enrichment of the host rocks in micas, and therefore in clay mineral precursors. This is an indication of lateral facies variation within the Loy Khwar Formation which,

as previously noted, shows considerable variation in thickness and mineralogy in the vicinity of the Aynak deposits.

5.4. Geochemical–mineralogical evidence for origin of the Aynak copper deposits

The geochemical–mineralogical associations indicate that Al, Fe and Ti, together with large ion lithophile and high field strength elements, were primary components of the precursor sediment, whereas copper plus additional sulphur and associated trace elements Se, As and Bi were introduced subsequently. Iron exhibits relatively constant down-hole trends, and a plausible interpretation is that iron was already present prior to mineralization of the host sediments, and much or all of this iron became incorporated into Cu-bearing sulphide minerals in the ore zone. Above and below the main ore zone, iron was incorporated into iron sulphides, now represented by pyrite and pyrrhotite. In gangue intervals and throughout the host rocks, iron was incorporated into dolomite and the Fe-bearing micas biotite and phlogopite.

The abundance of carbonate lithologies, and of graphite and pyrobitumen in pelitic rocks, indicates high biological productivity in the marine environment in which the precursor sediments were deposited. Pyrobitumen (shungite) is regarded as evidence of the former presence of hydrocarbons (oil and/or gas), which could have been a source of sulphur (sour gas) and a reductant for copper deposition as sulphides (Kirkham 1989). Apatite is a major component in some metasediments, which suggests that it formed as an autochthonous component. This phosphate enrichment likely relates to organic processes producing phosphate which accumulated on the sea bed and mineralized during diagenesis (Ruttenberg and Berner 1993). In samples from Western Aynak, phosphorus enrichment is associated with carbonates and with Mo–U enrichment.

In such organic-rich sediment, early diagenetic processes would have included microbial sulphate reduction and the formation of early diagenetic iron sulphides. Based on petrographic observations, the paragenetic sequence of sulphide minerals comprises an early, probably diagenetic pyrite which, in the central part of the Loy Khwar Formation, was largely replaced by ore-grade chalcopyrite and bornite mineralization. This mineralization is attributed to an influx, during later diagenesis while the sediment was still sufficiently permeable to allow fluid circulation, of Cu as cuprous chloride complexes in oxidized brines (Brown 1971, 2017; Rose 1989). The source of the copper, and other metals enriched in the ore, is uncertain but is likely to be the sedimentary

formations and voluminous volcanic rocks in the underlying (upper) Welayati Formation and/or the overlying Gulkhamid Formation that sandwich the Loy Khwar Formation. The volcanic rocks are predominantly mafic in composition which would hinder copper solubility unless they had been oxidized by subaerial weathering. The Logar ultramafic complex (indicated in Figure 1(c) by chromite and asbestos occurrences) cannot have been a Cu source as the intrusions post-date development of metamorphic fabrics in the Loy Khwar Formation.

As suggested by AGS and BGS (2005a), dolomitization of carbonate rocks in the sedimentary succession probably took place at the same time as copper sulphide mineralization, with Mg-rich evaporite-derived brines altering the precursor calcium carbonate to dolomite. This scenario is consistent with an equatorial location of the Aynak Block in the Cryogenian, and with evidence for relatively high concentrations of magnesium and sulphate in seawater at that time (Hitzman et al. 2010) which correlates with a global peak in the formation of sediment-hosted stratiform copper deposits (Parnell and Boyce 2019). Phosphorus derived from weathering of extensive mafic lavas is considered to have fertilized the Neoproterozoic oceans (Horton 2015).

In the Aynak deposit, further influxes of mineralizing fluids may have been associated with fracture permeability after lithification. Regional metamorphism resulted in the recrystallization and localized redistribution of sulphides, quartz and carbonates into segregations and fractures. Minor replacement of bornite by chalcopyrite, and of pyrrhotite by pyrite, took place during retrograde metamorphism.

5.5. Sulphur isotope evidence for origin of the Aynak copper deposits

In the interpretation of sulphur isotope values it is important to consider that significant mineral–fluid fractionations can take place during sulphide mineral deposition, particularly on reduction of sulphate to form sulphide minerals (Ripley and Ohmoto 1977). However, in this study, nearly all samples feature pyrite alongside chalcopyrite or bornite, and therefore sulphide or bisulphide would have dominated in solution and mineral–fluid fractionation is expected to be minimal (Barton 2014). The measured sulphide mineral $\delta^{34}S$ values are consequently taken to be representative of either the composition of primary sulphide mineral deposition in sediments, or of the hydrothermal fluids that precipitated or remobilized sulphide minerals.

Authors of sulphur isotope studies of sediment-hosted ore deposits commonly use the range of compositions to infer either thermochemical sulphate

reduction (TSR) or biogenic sulphate reduction (BSR) processes, or both, and hence consider whether the ore-forming processes were dominantly hydrothermal or dominantly sedimentary-diagenetic. However, there is considerable uncertainty as to the sulphate–sulphide isotopic fractionation factors applicable to TSR and BSR under various conditions. TSR yields sulphide with isotopic ratios that tend to be positive and are not too dissimilar to the isotopic ratios of the parent sulphate, for instance, at 160–180°C, an open system TSR should result in Δ^{34}

$S_{SO4\text{-sulphides}}$ of 12‰ to 14‰ (Machel et al. 1995; Rickard 2012). Conversely, fractionations over 20‰ are very unlikely to be due to thermochemical processes and are inferred to be biogenic in origin (Machel et al. 1995; Taylor and Beaudoin 2000).

Examples of the application of this logic are provided by sulphur isotope studies of the Central African Copperbelt deposits Nchanga, Luiswishi and Kamoto. In a study of the Nchanga deposit, McGowan et al. (2003) found that the δ^{34}S values of diagenetic pyrites within black shale range from –1 to –17‰, typical of biogenically reduced seawater sulphate, whereas the δ^{34}S values of copper sulphides range from –1 to +18‰, which they conclude are more representative of thermochemical reduction of sulphate-enriched fluid. Paragenetically late pyrite is characterized by

δ^{34}S values of +22 to +23‰, interpreted as indicating thermochemical reduction with limited fractionation of reduced sulphur relative to the parent sulphate. Similarly, for Luiswishi and Kamoto, El Desouky et al. (2010) conclude that BSR contributed sulphur to paragenetically early Cu-Co sulphides that have δ^{34}S values of –10.3 to +3.1‰, whereas TSR contributed sulphur to some paragenetically later sulphides that have δ^{34}S values of +18.6 to +21.0‰, comparable to contemporaneous Neoproterozoic seawater. Other second-stage Cu-Co sulphides have δ^{34}S values similar to those of the first stage (–13.1 to +5.2‰) and are interpreted by El Desouky et al. to have formed by remobilization of first-stage sulphides.

Although the range of δ^{34}S values obtained from Aynak (Figure 11) falls within the same range these Central African Copperbelt deposits, no consistent patterns are shown in the values from various sulphide species, or in sulphide samples from different textural contexts, geographic locations and stratigraphic levels. Distinguishing early diagenetic sulphides from later sulphides is difficult in Aynak samples because of subsequent metamorphism. The δ^{34}S values of sulphides in metamorphic segregations (–0.7 to +12.2‰; n = 10) and cross-cutting veins (–5.9 to +11.5‰; n = 15) show relatively small ranges tending towards high positive values of δ^{34}S, favouring a thermochemical origin. A proportion
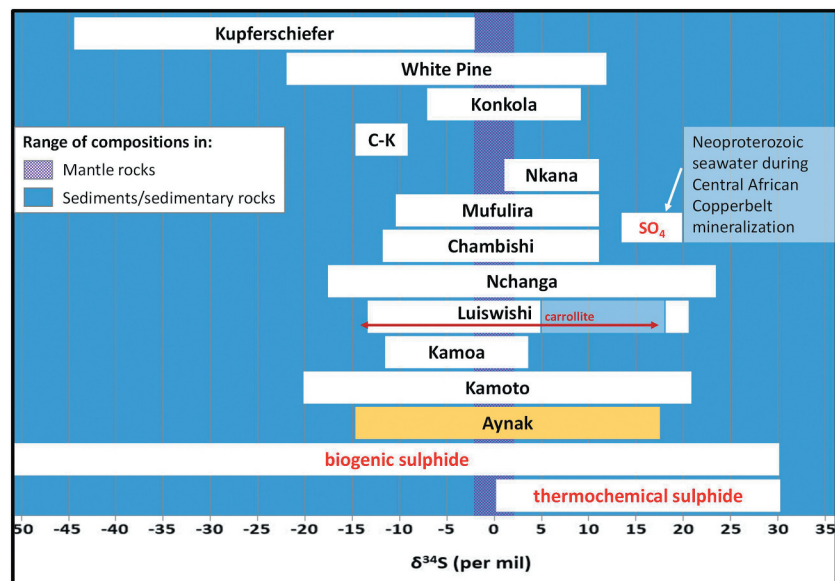
Figure 11. Ranges in δ^{34}S values for Central African Copperbelt and other worldwide sediment hosted copper deposits, compared to the range obtained for the Aynak deposit. Source of data: Kupferschiefer and White Pine (Gustafson and Williams 1981); C-K: Cheshmeh-Konan, Iran (Rajabpour et al. 2017); Konkola (Sweeney et al. 1986); Nkana North, Mufulira and Neoproterozoic seawater at the time of Lower Roan deposition (Claypool et al. 1980; Annels 1989); Chambishi (Annels 1989); Nchanga (McGowan et al. 2006); Luiswishi (El Desouky et al., with carrollite range from Lerouge et al. 2005); Kamoa, (Schmandt et al. 2013); Kamoto (El Desouky et al. 2010); Aynak (Waizy 2018). Also shown are ranges for biogenic and thermochemically produced sulphides, as suggested by Emery and Robinson (1993) and Machel et al. (1995), and for mantle- and sediment-hosted sulphur.

of the sulphur may conceivably have a mantle derivation (δ^{34}S ~0‰) via intrusive mafic igneous rocks, with low positive values indicating mixing with the thermochemical reduction of sulphate-enriched fluids. This hypothesis is compatible with the relatively narrow range and low positive tendency of δ^{34}S$_{sulfide}$ values from the potential 'copper source rocks' studied in the Khayarkhana area (Figure 1(c)). However, the strongly negative δ^{34}S values (–14.5 to –10.4‰) found in four Aynak sulphide samples are unlikely to have formed through thermochemical reduction processes. These isotope ratios are more likely due to biogenic reduction of seawater or porewater sulphate and could represent early diagenetic sulphide–sulphur.

The biogenic reduction of seawater sulphate, or of sediment porewater sulphate, is considered to have been a key process in the formation of many stratabound sulphide deposits including sediment-hosted copper deposits (Brown 1997; Bechtel et al. 2001; El Desouky et al. 2010; Shanks 2014). These deposits commonly show wide ranges of δ^{34}S$_{sulfide}$ values, for instance, sulphides in the Mesoproterozoic White Pine deposit range from –22 to +12‰, and those in the Upper Permian Kupferschiefer in Eastern Europe range from –44 to –2‰ (Figure 11).

In a petrographic and sulphur isotope study of the Konkola stratiform Cu–Co deposit in Zambia, Torremans et al. (2013) obtained δ^{34}S values for chalcopyrite in the range –8.7 to +1.4‰. If it is considered that the sulphides formed by reduction of contemporaneous seawater sulphate, the reported fractionation values of between 18.6 and 25.5‰ are consistent with biogenic sulphate reduction in a relatively closed environment (cf. Machel 2001). Torremans et al. (2013) propose that localized remobilization of sulphur from early diagenetic sulphides led to the observed δ^{34}S similarities of disseminated, lensoid and vein sulphides at Konkola. This isotopic homogeneity contrasts with Nchanga and Kamoa where diagenetic pyrite has δ^{34}S values different from that of copper sulphides in the orebodies, indicating the involvement of different reduction processes, namely BSR and TSR respectively (McGowan et al. 2003). The Kamoa deposit has a narrow range of sulphur isotope ratios in ore-stage sulphides (Figure 11), and Schmandt et al. (2013) suggest that Kamoa represents a single pulse of intense copper mineralization, rather than the multistage mineralization processes that generate a broad range in sulphur isotope compositions, illustrated for example by the nearby Kamora deposit (El Desouky et al. 2010).

A large range of δ^{34}S$_{sulfide}$ values from –14.4 to +17.5‰ was found by Lerouge et al. (2005) in carrollite ($CuCo_2S_4$) from the Neoproterozoic Luiswishi Cu–Co ore deposits in Congo (Figure 11). The authors conclude that the distribution of δ^{34}S values indicate a strong stratigraphic control of the sulphur isotope signature, supporting a model based on biogenic sulphate reduction during early diagenesis of the host sediments deposited in a shallow marine to lacustrine environment. An upward decrease of δ^{34}S values is consistent with lithological evidence for a transgressive–regressive evolution of the ore-hosting sedimentary sequence (Cailteux 1994) with deposition of copper sulphides during a period of regression in a basin isolated from the ocean.

As noted above, whereas sulphides in the Aynak deposit show a wide range in δ^{34}S values, these do not show simple and consistent stratigraphic trends, the absence of which argues against their origin through predominantly biogenic reduction processes. Consequently we favour a dual origin, as indicated in Figure 12, whereby some of the sulphide incorporated synsedimentary or early diagenetic sulphur produced by BSR, whereas other sulphides, formed paragenetically later and associated with hydrothermal alteration, incorporated sulphur generated by TSR processes. In this respect, the Aynak deposit appears to have formed in a manner similar to Nchanga and other Central African Copperbelt deposits (McGowan et al. 2003; El Desouky et al. 2010).

6. Conclusions

Regional metamorphism to lower amphibolite facies (garnet grade) clearly had a profound effect on the mineralogy and textures of the Aynak ore and sedimentary host rocks, generating coarsely crystalline sulphide rocks and marbles. Nevertheless, relatively fine grain sizes are widely preserved perhaps due to the inhibition of recrystallization (under these conditions) by micron-sized inclusions of graphite and sulphides. In these fine-grained rocks (now marble, quartzite and quartz-carbonate-mica schist), sedimentary lamination is preserved with bedding-parallel disseminated sulphides which contain microscopic relicts of diagenetic textures, notably inclusion-rich anhedral pyrite. Some samples preserve evidence that this early pyrite has been partially replaced by chalcopyrite. Widespread and locally abundant graphite, pyrobitumen and apatite attest to the high organic productivity in the depositional environment. The predominance of dolomite over calcite, and association of pyrobitumen with dolomite in some rocks, is consistent with extensive dolomitization during diagenesis. In the Western Aynak deposit, chlorine
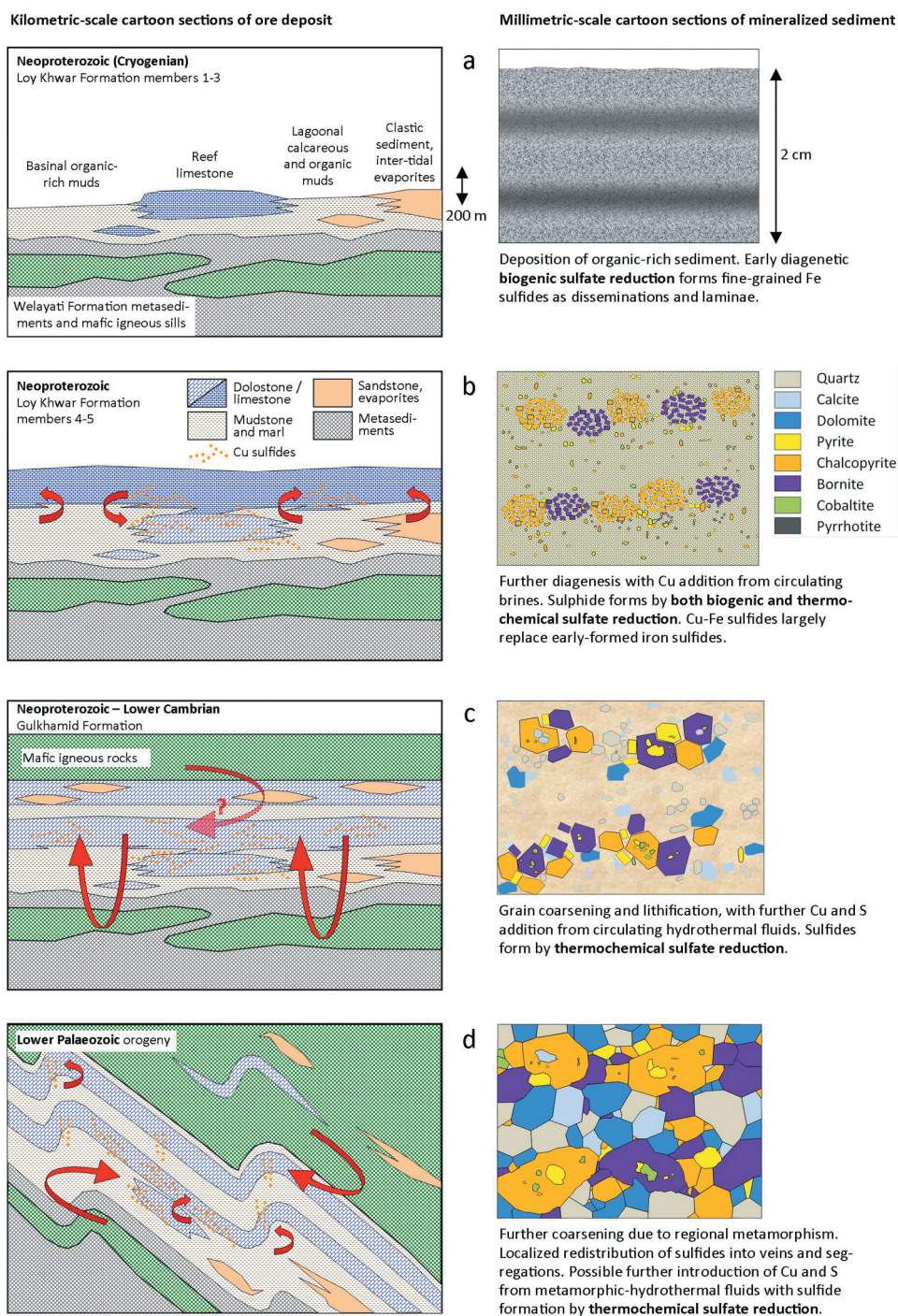
Kilometric-scale cartoon sections of ore deposit

Millimetric-scale cartoon sections of mineralized sediment

Neoproterozoic (Cryogenian)
Loy Khwar Formation members 1-3

Basinal organic-rich muds
Reef limestone
Lagoonal calcareous and organic muds
Clastic sediment, inter-tidal evaporites
200 m

Welayati Formation metasediments and mafic igneous sills

a
2 cm

Deposition of organic-rich sediment. Early diagenetic **biogenic sulfate reduction** forms fine-grained Fe sulfides as disseminations and laminae.

Neoproterozoic
Loy Khwar Formation members 4-5

Dolostone / limestone
Sandstone, evaporites
Mudstone and marl
Metasediments
Cu sulfides

b

Quartz
Calcite
Dolomite
Pyrite
Chalcopyrite
Bornite
Cobaltite
Pyrrhotite

Further diagenesis with Cu addition from circulating brines. Sulphide forms by **both biogenic and thermochemical sulfate reduction**. Cu-Fe sulfides largely replace early-formed iron sulfides.

Neoproterozoic – Lower Cambrian
Gulkhamid Formation

Mafic igneous rocks

?

c

Grain coarsening and lithification, with further Cu and S addition from circulating hydrothermal fluids. Sulfides form by **thermochemical sulfate reduction**.

Lower Palaeozoic orogeny

d

Further coarsening due to regional metamorphism. Localized redistribution of sulfides into veins and segregations. Possible further introduction of Cu and S from metamorphic-hydrothermal fluids with sulfide formation by **thermochemical sulfate reduction**.

Figure 12. Genetic model for the Aynak copper deposits. Four stages (a–d) are represented, in each case with kilometric-scale (left) and millimetric-scale (right) vertical sections illustrating the stratigraphic and textural development of the orebodies. The first stage kilometric-scale section is modified from a diagram by AGS and BGS (2005a).

enrichment in apatite and occurrences of scapolite indicate the former presence of evaporates in this area.

Geochemical trends in the sample set concur with stratigraphic and petrographic observations which indicate that oxidized metalliferous brines permeated through the organic-rich (low Eh) sediments of the Loy Khwar Formation, and interacted with pre-existing iron sulphides to precipitate Cu- and Co-rich sulphides. This interaction, as modelled by Muchez and Corbella (2012), produced zoned orebodies with the central bornite-rich zone representing the most intense copper mineralization and the adjacent chalcopyrite and peripheral pyrite zones

representing progressively less intense mineralization. Subaerially weathered mafic volcanic rocks overlying and/or underlying the Loy Khwar Formation sediments were probably the source of Cu, Se, Co and Bi in the circulating brines (Figure 12), although this source was not convincingly established by the methods in this study.

The broad range of $\delta^{34}S$ values (−14.5 to +17.3‰) in disseminated and bedding-parallel sulphides from Aynak, as well as the considerable decimetre to metre scale variations of $\delta^{34}S$ values, support a formation process involving the biogenic reduction of seawater/porewater sulphate during diagenesis of the host sediments, combined with thermochemical reduction during subsequent lithification and metamorphism (Figure 12). The somewhat narrower range of $\delta^{34}S$ values (−5.9 to +11.5‰) in sulphides from veins and metamorphic segregations, and similarity in S isotope compositions of adjacent stratabound and vein sulphides, suggest localized homogenization during regional metamorphism and deformation. Mafic basement rocks such as exposed in the Khayarkhana area may have provided a source of copper to circulating hydrothermal fluids. However, mafic rocks are unlikely to have contributed much sulphur to the Aynak deposit which is characterized by a considerably wider range of S isotope compositions including strongly negative values that are absent from the Khayarkhana samples. Strongly negative $\delta^{34}S$ values in some sulphides from Aynak suggest closed system fractionation during biogenic reduction of porewater sulphate, whereas strongly positive $\delta^{34}S$ values indicate sulphur derived directly from thermochemical reduction of sulphate, perhaps dissolved from evaporites that previously existed in the sedimentary sequence (Figure 12).

Overall our results support a multi-stage, sedimentary–diagenetic–hydrothermal genetic model for the Aynak ore deposit which is similar to that proposed for several of the Central African Copperbelt orebodies. Mineral textures (Figure 12) and sulphur isotope and bulk geochemical data do not favour either an exclusively syn-diagenetic model, or an exclusively epigenetic–metamorphic model. It is likely that Aynak is another example of the giant sediment-hosted copper deposits that formed worldwide in the Cryogenian period, associated with magnesium- and sulphate-rich seawater (Hitzman *et al.* 2010) and marine enrichment in copper coincident with profuse basaltic volcanism, oxidation of the oceans and the rise of metazoans (Parnell and Boyce 2019).

Disclosure statement

No potential conflict of interest was reported by the authors.

ORCID

Norman R. Moles http://orcid.org/0000-0003-1399-9709

References

AGS and BGS, 2005a, Aynak information package, part i introduction. Afghanistan: Geological Survey and British Geological Survey. www.bgs.ac.uk/AfghanMinerals/DMA_tender_docs.htm

AGS and BGS, 2005b, Aynak information package, part ii geological setting of Aynak and summary of exploration. Afghanistan: Geological Survey and British Geological Survey. https://www.bgs.ac.uk/AfghanMinerals/DMA_tender_docs.htm

Akocdzhanyan, L.A., Kryukov, Y.A., Zagordodniy, G.G., Kashin, A.A., Koloskov, V.P., Kubatkin, L.V., Makimov, T.M., Nevretdinov, E.B., Novosolcev, V.M., Sulikayev, K.I., and Cvetkov, L.P., 1977, Preliminary report on results of geological exploration of Aynak copper deposit in 1974–1976: English Version by Afghanistan Geological Survey and British Geological Survey. www.bgs.ac.uk/AfghanMinerals/DMA_tender_docs.htm

Annels, A.E., 1989, Ore genesis in the Zambian Copperbelt, with particular reference to the northern sector of the Chambishi Basin, in Boyle, R.W., Brown, A.C., Jefferson, C.W., Jowett, E.C., and Kirkham, R.V., eds., Sediment–hosted stratiform copper deposits, Volume 36. Canada: Geological Association of Canada Special Paper, p. 427–452.

Bailie, R., and Gutzmer, J., 2011, Age and primary architecture of the Copperton Zn-Cu VMS deposit, Northern Cape Province, South Africa: Ore Geology Reviews, v. 39, no. 3, p. 164–179. doi:10.1016/j.oregeorev.2011.02.001

Barton, M.D., 2014, Iron Oxide (–Cu–Au–REE–P–Ag–U–Co) Systems, in Treatise on Geochemistry, Volume 13 (Second edition): Elsevier Inc, p. 515–541. doi:10.1016/B978-0-08-095975-7.01123-2

Bechtel, A., Sun, Y., Puettmann, W., Hoernes, S., and Hoefs, J., 2001, Isotopic evidence for multi-stage base metal enrichment in the Kupferschiefer from the Sangerhausen Basin, Germany: Chemical Geology, v. 176, no. 1–4, p. 31–49. doi:10.1016/S0009-2541(00)00336-3

Benham, A.J., Coats, S., Kovac, P. and Norton, G., 2007, Aynak: a world-class sediment-hosted copper deposit, Afghanistan (conference presentation). Society for Mining, Metallurgy and Exploration, Denver, USA, 25–28 Feb 2007 (unpublished).

Bernstein, L.R., and Cox, D.P., 1986, Geology and sulfide mineralogy of the Number One orebody, Ruby Creek copper deposit, Alaska: Economic Geology, v. 81, no. 7, p. 1675–1689. doi:10.2113/gsecongeo.81.7.1675

Brown, A.C., 1971, Zoning in the White Pine copper deposit, Ontonagon County, MI, USA: Economic Geology, v. 66, no. 4, p. 543–573. doi:10.2113/gsecongeo.66.4.543

Brown, A.C., 1997, World-class sediment-hosted stratiform copper deposits: Characteristics, genetic concepts and metallotects: Australian Journal of Earth Sciences, v. 44, p. 317–328.

Brown, A.C., 2017, Constraints on conceptual and quantitative modelling of early diagenetic sediment-hosted stratiform copper mineralization: Minerals, v. 7, no. 10, p. 192–204. doi:10.3390/min7100192

Cailteux, J., 1994, Lithostratigraphy of the Neoproterozoic Shaba-type (Zaire) Roan Supergroup and metallogenesis of associated stratiform mineralization. In Kampunzu AB, Lubala RT (editors), Neoproterozoic Belts of Zambia, Zaire and Namibia: Journal of African Earth Sciences, v. 19, no. 4, p. 279–301. doi:10.1016/0899-5362(94)90015-9

Cailteux, J.L.H., Kampunzu, A.B., Lerouge, C., Kaputo, A.K., and Milesi, J.P., 2005, Genesis of sediment-hosted stratiform copper–cobalt deposits, central African Copperbelt: Journal of African Earth Sciences, v. 42, no. 1–5, p. 134–158. doi:10.1016/j.jafrearsci.2005.08.001

Carlson, W.D., 2011, Porphyroblast crystallization: Linking processes, kinetics, and microstructures: International Geology Review, v. 53, no. 3–4, p. 406–445. doi:10.1080/00206814.2010.496184

Cartwright, I., and Oliver, N.H.S., 2000, Metamorphic fluids and their relationship to the formation of metamorphosed and metamorphogenic ore deposits: Reviews in Economic Geology, v. 11, p. 81–96.

Chisonga, B.C., Gutzmer, J., Beukes, N.J., and Huizenga, J.M., 2012, Nature and origin of the protolith succession to the Paleoproterozoic Serra do Navio manganese deposit, Amapa Province, Brazil: Ore Geology Reviews, v. 47, p. 59–76. doi:10.1016/j.oregeorev.2011.06.006

Claypool, G.E., Holser, W.T., Kaplan, I.R., Sakai, H. and Zak, I., 1980, The age curves of sulfur and oxygen isotopes in marine sulfate and their mutual interpretation. Chemical Geology, v. 28, p. 199–260.

Collett, S., Faryad, S.W., and Mosazai, A.M., 2015, Polymetamorphic evolution of the granulite-facies Paleoproterozoic basement of the Kabul Block, Afghanistan: Mineralogy and Petrology, v. 109, no. 4, p. 463–484. doi:10.1007/s00710-015-0371-9

Craig, D., 2013, A technical report on the Taghar Drilling Program, North Aynak Copper Province, Afghanistan. SRK Consulting Project Number 378700.010.

Craig, J.R., and Vokes, F.M., 1993, The metamorphism of pyrite and pyritic ores: An overview: Mineralogical Magazine, v. 57, p. 3–18.

Crowe, D.E., Valley, J.W., and Baker, K.L., 1990, Micro–analysis of sulfur–isotope ratios and zonation by laser microprobe: Geochimica et Cosmochimica Acta, v. 54, p. 2075–2092.

Deer, W.A., Howie, R.A., Wise, W.S. and Zussman, J., 2004, Rock-forming minerals. Volume 4B (second edition) Framework silicates: Silica minerals, feldspathoids and the zeolites. The Geological Society of London, p.982

El Desouky, H.A., Muchez, P., Boyce, A.J., Schneider, J., Cailteux, J.L.H., Dewaele, S., and Quadt, A., 2010, Genesis of sediment-hosted stratiform copper–cobalt mineralization at Luiswishi and Kamoto, Katanga Copperbelt (Democratic Republic of Congo): Mineralium Deposita, v. 45, no. 8, p. 735–763. doi:10.1007/s00126-010-0298-3

El Desouky, H.A., Muchez, P., Dewaele, S., Boutwood, A., and Tyler, R., 2008, Post-orogenic origin of the stratiform Cu mineralization at Lufukwe, Lufilian Foreland, Democratic Republic of Congo: Economic Geology, v. 103, no. 3, p. 555–582. doi:10.2113/gsecongeo.103.3.555

Emery, D., and Robinson, A. 1993, Inorganic Chemistry: Applications to Petroleum Geology: Oxford, Blackwell Science Publication, p. 254p.

Faryad, S.W., Collett, S., Finger, F., Sergeev, S.A., Čopjaková, R., and Simon, P., 2016, The Kabul Block (Afghanistan), a segment of the Columbia supercontinent, with a Neoproterozoic metamorphic overprint: Gondwana Research, v. 34, p. 221–240. doi:10.1016/j.gr.2015.02.019

Feruz, N.M., 1973, The geological structure of the Kabul Tectonic Zone (Afghanistan). PhD thesis, Moscow State University, Moscow.

Fontbote, L., Kouzmanov, K., Chiaradia, M., and Pokrovski, G.S., 2017, Sulfide minerals in hydrothermal deposits: Elements, v. 13, no. 2, p. 97–103. doi:10.2113/gselements.13.2.97

Giacometti, F., Evans, K.A., Rebay, G., Cliff, J., Tomkins, A.G., Rossetti, P., Vaggelli, G., and Adams, D.T., 2014, Sulfur isotope evolution in sulfide ores from Western Alps: Assessing the influence of subduction-related metamorphism: Geochemistry, Geophysics, Geosystems, v. 15, no. 10, p. 3808–3829. doi:10.1002/2014GC005459

Gusev, I.A., Safonov, B.A., et al., 1979, Geological structure of the Kabul copper ore field: AGS Archive, Kabul, Afghanistan.

Gustafson, L.B., and Williams, N., 1981, Sediment–hosted stratiform deposits of copper, lead and zinc: Economic Geology, 75th Anniversary Volume, v. 5, p. 138–178.

Hall, A.J., Boyce, A.J., and Fallick, A.E., 1987, Iron sulfides in metasediments: Isotopic support for a retrogressive pyrrhotite to pyrite reaction: Chemical Geology (Isotope Geoscience Section), v. 65, no. 3–4, p. 305–310. doi:10.1016/0168-9622(87)90010-8

Hitzman, M.W., Kirkham, R., Broughton, D., Thorson, J., and Selley, D., 2005, The sediment-hosted stratiform copper ore system: Economic Geology, 100th Anniversary Volume, p. 609–642.

Hitzman, M.W., Proffett, J.M., Jr, Schmidt, J.M., and Smith, T.E., 1986, Geology and mineralization of the Ambler district, northwestern Alaska: Economic Geology, v. 81, no. 7, p. 1592–1618. doi:10.2113/gsecongeo.81.7.1592

Hitzman, M.W., Selley, D., and Bull, S., 2010, Formation of sedimentary rock-hosted stratiform copper deposits through Earth history: Economic Geology, v. 105, no. 3, p. 627–639. doi:10.2113/gsecongeo.105.3.627

Horton, F., 2015, Did phosphorus derived from the weathering of large igneous provinces fertilize the Neoproterozoic ocean?: Geochemistry, Geophysics, Geosystems, v. 16, no. 6, p. 1723–1738. doi:10.1002/2015GC005792

Kirkham, R.V., 1989, Distribution, settings, and genesis of sediment-hosted stratiform copper deposits, in Boyle, R.W., Brown, A.C., Jefferson, C.W., Jowett, E.C., and Kirkham, R.V., eds., Sediment-hosted stratiform copper deposits. Canada: Geological Association of Canada special paper 36, p. 3–38.

Large, R.R., Gemmell, J.B., Paulick, H., and Huston, D.L., 2001, The Alteration Box Plot: A simple approach to understanding the relationship between alteration mineralogy and lithogeochemistry associated with volcanic-hosted massive sulfide deposits: Economic Geology, v. 96, p. 957–971.

Lerouge, C., Cailteux, J., Kampunzu, A.B., Milesi, J.P., and Flehoc, C., 2005, Sulphur isotope constraints on formation conditions of the Luiswishi deposits ore, Democratic Republic of Congo (DRC): Journal of African Earth Sciences, v. 42, no. 1–5, p. 173–182. doi:10.1016/j.jafrearsci.2005.08.004

Li, K., Brugger, J., and Pring, A., 2018, Exsolution of chalcopyrite from bornite-digenite solid solution: An example of a fluid-driven back-replacement reaction: Mineralium Deposita, v. 53, no. 7, p. 903–908. doi:10.1007/s00126-018-0820-6

Lipfert, G., Sidle, W.C., Reeve, A.S., Ayuso, R.A., and Boyce, A.J., 2007, High arsenic concentration and enriched sulfur and oxygen isotopes in a fractured–bedrock groundwater system: Chemical Geology, v. 242, no. 3–4, p. 385–399. doi:10.1016/j.chemgeo.2007.04.003

Ludington, S., Orris, G.J., Bolm, K.S., and Peter, S.G., 2007, US geological survey-Afghanistan ministry of mines and industry joint mineral resource assessment team, preliminary mineral resource assessment of selected mineral deposit types in Afghanistan: U.S. Geological Survey Report Series 2007-1005, p. 44.

Machel, H.G., 2001, Bacterial and thermochemical sulfate reduction in diagenetic settings – Old and new insights: Sedimentary Geology, v. 140, no. 1–2, p. 143–175. doi:10.1016/S0037-0738(00)00176-7

Machel, H.G., Krouse, H.R., and Sassen, R., 1995, Products and distinguishing criteria of bacterial and thermochemical sulfate reduction: Applied Geochemistry, v. 10, no. 4, p. 373–389. doi:10.1016/0883-2927(95)00008-8

Mandeville, C.W., 2010, Sulfur: A ubiquitous and useful tracer in Earth and planetary sciences: Elements, v. 6, no. 2, p. 75–80. doi:10.2113/gselements.6.2.75

Marignac, C., Diagana, B., Cathelineau, M., Boiron, M., Banks, D., Fourcade, S., and Vallance, J., 2003, Remobilisation of base metals and gold by Variscan metamorphic fluids in the south Iberian pyrite belt: Evidence from the Tharsis VMS deposit: Chemical Geology, v. 194, no. 1–3, p. 143–165. doi:10.1016/S0009-2541(02)00275-9

Marshall, B., Vokes, F.M., and Larocque, A.C.L., 2000, Regional metamorphic remobilization: Upgrading and formation of ore deposits: Reviews in Economic Geology, v. 11, p. 19–38.

Mathieu, L., 2018, Quantifying hydrothermal alteration: A review of methods: Geosciences, v. 8, no. 7, p. 245–272. doi:10.3390/geosciences8070245

McGowan, R.R., Roberts, S., Foster, R.P., Boyce, A.J., and Coller, D., 2003, Origin of the copper-cobalt deposits of the Zambian Copperbelt: An epigenetic view from Nchanga: Geology, v. 31, no. 6, p. 497–500. doi:10.1130/0091-7613-(2003)031<0497:OOTCDO>2.0.CO;2

Mennesier, G., 1961, Les caracteres structuraux des montagnes de la region de Kaboul (Afghanistan): Kabul, Afghanistan (in French), Afghanistan Geological Survey Archive.

MOMP and AGS, 2014, Copper of Afghanistan, in Ministry of Mines and Petroleum and Afghanistan Geological Survey, Minerals in Afghanistan. http://mom.gov.af/Content/files/MOMP_COPPER_%20Midas_Jan_2014_LATEST.pdf

Muchez, P., and Corbella, M., 2012, Factors controlling the precipitation of copper and cobalt minerals in sediment-hosted ore deposits: Advances and restrictions: Journal of Geochemical Exploration, v. 118, p. 38–46. doi:10.1016/j.gexplo.2012.04.006

Muirhead, D.K., Parnell, J., Spinks, S., and Bowden, S.A., 2016, Characterization of organic matter in the Torridonian using Raman spectroscopy, in Brasier, A.T., McIlroy, D., and McLoughlin, N., eds., Earth system evolution and early life: A celebration of the work of Martin Brasier: Geological Society, London, Special Publications, Vol. 448, p. 71–80. doi:10.1144/SP448.2

Oummouch, A., Essaifi, A., Zayane, R., Maddi, O., Zouhair, M., and Maacha, L., 2017, Geology and metallogenesis of the sediment-hosted Cu-Ag deposit of Tizert (Igherm Inlier, Anti-Atlas Copperbelt, Morocco): Geofluids, v. 2017, Article ID 7508484, p. 19. doi:10.1155/2017/7508484

Parnell, J., and Boyce, A.J., 2019, Neoproterozoic copper cycling, and the rise of metazoans: Nature Scientific Reports, v. 9, no. 3638, p. 1–7.

Perelló, J., Clifford, J.A., Creaser, R.A., and Valencia, V.A., 2015, An example of synorogenic sediment-hosted copper mineralization: Geologic and geochronologic evidence from the Paleoproterozoic Nussir deposit, Finnmark, Arctic Norway: Economic Geology, v. 110, no. 3, p. 677–689. doi:10.2113/econgeo.110.3.677

Raiswell, R., Reinhard, C.T., Derkowski, A., Owens, J., Bottrell, S. H., Anbar, A.D., and Lyons, T.W., 2011, Formation of syngenetic and early diagenetic iron minerals in the late Archean Mt. McRae Shale, Hamersley Basin, Australia: New insights on the patterns, controls and paleoenvironmental implications of authigenic mineral formation: Geochimica et Cosmochimica Acta, v. 75, p. 1072–1087.

Rajabpour, S., Abedini, A., Alipour, S., Lehmann, B., and Jiang, S.-Y., 2017, Geology and geochemistry of the sediment-hosted Cheshmeh-Konan redbed-type copper deposit, NW Iran: Ore Geology Reviews, v. 86, p. 154–171. doi:10.1016/j.oregeorev.2017.02.013

Rickard, D., 2012, Chapter 13 Euxinic Systems, in Sulfidic sediments and sedimentary rocks: Developments in Sedimentology, v. 65, p. 495–542.

Ripley, E.M., and Ohmoto, H., 1977, Mineralogic, sulphur isotope, and fluid inclusion studies of the stratabound copper deposits at the Raul Mine, Peru: Economic Geology, v. 72, no. 6, p. 1017–1041. doi:10.2113/gsecongeo.72.6.1017

Robinson, B.W., and Kusakabe, M., 1975, Quantitative preparation of SO_2 for $^{34}S/^{32}S$ analysis from sulphides by

combustion with cuprous oxide: Analytical Chemistry, v. 47, no. 7, p. 1179–1181. doi:10.1021/ac60357a026

Rose, A.W., 1989, Mobility of copper and other heavy metals in sedimentary environments, in Boyle, R.W., Brown, A.C., Jefferson, C.W., Jowett, E.C., and Kirkham, R.V., eds., Sediment-Hosted Stratiform Copper deposits: Geological Association of Canada special paper 36, p. 97–110.

Ruttenberg, K.C., and Berner, R.A., 1993, Authigenic apatite formation and burial in sediments from non-upwelling, continental margin environments: Geochimica et Cosmochimica Acta, v. 57, p. 991–1007.

Sangster, D.F., 2018, Toward an integrated genetic model for vent-distal SEDEX deposits: Mineralium Deposita, v. 53, no. 4, p. 509–527. doi:10.1007/s00126-017-0755-3

Schmandt, D., Broughton, D., Hitzman, M.W., Plink-Bjorklund, P., Edwards,D. and Humphrey, J., 2013, The Kamoa Copper Deposit, Democratic Republic of Congo: Stratigraphy, diagenetic and hydrothermal alteration, and mineralization. Economic Geology, v. 108, p. 1301–1324

Selby, D., Kelley, K.D., Hitzman, M.W., and Ziec, J., 2009, Re-Os sulfide (bornite, chalcopyrite, and pyrite) systematics of the carbonate-hosted copper deposits at Ruby Creek, Southern Brooks Range, Alaska: Economic Geology, v. 104, no. 3, p. 437–444. doi:10.2113/gsecongeo.104.3.437

Selley, D., Broughton, D., Scott, R., Hitzman, M., Bull, S., Large, R., McGoldrick, P., Croaker, M., Pollington, N., and Barra, F., 2005, A new look at the geology of the Zambian Copperbelt: Economic Geology, 100th Anniversary Volume, p. 965–1000.

Shanks, W.C.P., 2014, Stable isotope geochemistry of mineral deposits, in Treatise on Geochemistry (2nd edition): Amsterdam, Elsevier, p. 59–85.

Sillitoe, R.H., Perelló, J., and Garćia, A., 2010, Sulfide-bearing veinlets throughout the stratiform mineralization of the Central African Copperbelt: Temporal and genetic implications: Economic Geology, v. 105, no. 8, p. 1361–1368. doi:10.2113/econgeo.105.8.1361

Sillitoe, R.H., Perello, J., Creaser, R.A., Wilton, J., Wilson, A.J., and Dawborn, T., 2017, Age of the Zambian Copperbelt: Mineralium Deposita, v. 52, p. 1245–1268.

Skala, W., 1979, Some effects of the constant-sum problem in geochemistry: Chemical Geology, v. 27, no. 1–2, p. 1–9. doi:10.1016/0009-2541(79)90099-8

Slavin, V.I., Fedorov, T.O., and Feroz, N.M., 1972, The geology and age of the metamorphic complex in the Kabul District: Moscow, Vestnik MSU.

Sweeney, M.A., Turner, P., and Vaughan, D.J., 1986, Stable isotope and geochemical studies of the role of early digenesis in ore formation, Konkola Basin, Zambian Copperbelt: Economic Geology, v. 81, p. 1836–1852.

Taylor, B.E., and Beaudoin, G., 2000, Sulphur stratigraphy of the Sullivan Pb–Zn –Ag deposit, B.C: Evidence for hydrothermal sulphur, and bacterial and thermochemical sulphate reduction, in Lydon, J.W., Ho¨y, T., Slack, J.F., and Knapp, M., eds., The sullivan deposit and its geological environment. Special Publication, Volume 1: St. John's, Newfoundland, Mineral Deposits Division of the Geological Association of Canada, p. 696–719.

Taylor, C.D., Causey, J.D., Denning, P.D., Hammarstrom, J.M., Hayes, T.S., Horton, J.D., Kirschbaum, M.J., Parks, H.L., Wilson, A.B., Wintzer, N.E., and Zientek, M.L., 2013, Descriptive models, grade-tonnage relations, and databases for the assessment of sediment-hosted copper deposits with emphasis on deposits in the Central African Copperbelt, Democratic Republic of the Congo and Zambia: U.S. Geological Survey Scientific Investigations Report 2010–5090–J, 154 p. and data files.

Torremans, K., Gauquie, J., Boyce, A.J., Barrie, C.D., Sikazwe, O., and Muchez, P.H., 2013, Remobilisation features and structural control on ore grade distribution at the Konkola stratiform Cu–Co ore deposit, Zambia: Journal of African Earth Sciences, v. 79, p. 10–23.

Turlin, F., Eglinger, A., Vanderhaeghe, O., André-Mayer, A.S., Poujol, M., Mercadier, J., and Bartlett, R., 2016, Synmetamorphic Cu remobilization during the Pan-African orogeny: Microstructural, petrological and geochronological data on the kyanite-micaschists hosting the Cu (–U) Lumwana deposit in the Western Zambian Copperbelt of the Lufilian belt: Ore Geology Reviews, v. 75, p. 52–75.

Van Gaans, P.F.M., Vriend, S.P., and Schuiling, R.D., 1986, Integral Rock Analysis: A new approach in lithogeochemical exploration with use of X-ray fluorescence spectrometry: Geologie Und Mijnbouw, v. 65, p. 205–213.

Velasco, F., Sanchez–Espana, J., Boyce, A.J., Fallick, A.E., Saez, R., and Almodovar, G.R., 1998, A new sulphur isotopic study of some Iberian Pyrite Belt deposits: Evidence of a textural control on sulphur isotope composition: Mineralium Deposita, v. 34, p. 4–18.

Waizy, H., 2018, Geology and genesis of the Aynak Copper Deposits in the Kabul Basin, Afghanistan [PhD thesis]: UK, University of Brighton, 230 p.

Wilkinson, J.J., 2014, Sediment-hosted zinc-lead mineralization, in Holland, H., and Turekian, K., eds., Treatise on Geochemistry, Volume 13: Elsevier, p. 219–249.

Wopenka, B., and Pasteris, J.D., 1993, Structural characterization of kerogens to granulite-facies graphite: Applicability of Raman microprobe spectroscopy: American Mineralogist, v. 78, p. 533–557.

Yund, R.A., and Kullerud, G., 1966, Thermal stability of assemblages in the Cu-Fe-S system: Journal of Petrology, v. 7, p. 454–488.

Yurgenson, G.A., Akram, A.M., Dzhelani, K.G., and Gavrilov, A.M., 1981, Mineralnyye tipy rud I posledovatel'nost' obrazovaniya sul'fidov na mestorozhdenii medi Aynak (Respublika Afganistan), [Type minerals of ores and sulfide sequence in Aynak copper deposit, Afghanistan]: Izvestiya Vysshikh Uchebnykh Zavedeniy, Geologiya I Razvedka, v. 1981, no. 6, p. 150–153.

Zhang, Y., Gao, J.-F., Ma, D., and Pan, J., 2018, The role of hydrothermal alteration in tungsten mineralization at the Dahutang tungsten deposit, South China: Ore Geology Reviews, v. 95, p. 1008–1027.

Zheng, L., Chen, Y.J., Pete, H., and Chen, H.Y., 2013, Metamorphosed Pb-Zn-(Ag) ores of the Keketale VMS deposit, Xinjiang: Evidence from ore textures, fluid inclusions, geochronology and pyrite compositions: Ore Geology Reviews, v. 54, p. 167–180.

Zhong, R.C., Li, W.B., Chen, Y.J., Ji, J.Q., Hu, C.S., Yang, Y.F., and Hu, C., 2015, Significant Zn-Pb-Cu remobilization of a syngenetic stratabound deposit during regional metamorphism: A case study in the giant Dongshengmiao deposit, northern China: Ore Geology Reviews, v. 64, p. 89–102.